Less sensitive proton-exchange membrane to a relative humidity below 30%

Sahng Hyuck Woo, Belkacem Otazaghine, Sara Cavaliere, Byeong-Seon An, Hee Soo Kim, Jae-Hun Kim, Young-Gi Yoon, Soo Youn Lee, Arnaud Rigacci, Christian Beauger

Less sensitive proton-exchange membrane to a relative humidity below 30%

Sahng Hyuck Woo [a,b,*], Belkacem Otazaghine [c], Sara Cavaliere [d], Byeong-Seon An [e], Hee Soo Kim [f], Jae-Hun Kim [b], Young-Gi Yoon [g], Soo Youn Lee [b], Arnaud Rigacci [a], Christian Beauger [a,**]

[a] MINES Paris, PSL University, Center for Processes, Renewable Energy and Energy Systems (PERSEE), CS 10207 rue Claude Daunesse, F-06904, Sophia Antipolis Cedex, France
[b] Gwangju Clean Energy Research Center, Korea Institute of Energy Research (KIER), 270-25 Samso-ro, Gwangju, 61003, Republic of Korea
[c] Polymers Composites and Hybrids (PCH), IMT Mines Ales, Ales Cedex, France
[d] Institut Charles Gerhardt, UMR, CNRS 5253, Agrégats Interfaces et Matériaux pour l'Energie, Université de Montpellier, 34095, Montpellier Cedex 5, France
[e] Analysis Center for Energy Research, Korea Institute of Energy Research (KIER), Daejeon, 34129, Republic of Korea
[f] Green Materials & Processes R&D Group, Korea Institute of Industrial Technology, Ulsan, 44413, Republic of Korea
[g] Fuel Cell Research and Demonstration Center, Hydrogen Energy Research Division, Korea Institute of Energy Research (KIER), Buan-gun, Jeollabuk-do, 56332, Republic of Korea

A B S T R A C T

In this work, we focus on a novel sepiolite-incorporated Aquivion composite membrane that can be operated in a proton-exchange membrane fuel cell (PEMFC) at a relative humidity (RH) below 30%. The maximum power density reduction of the developed membrane is only 0.77% at 30% RH. In the study, we demonstrated adding sepiolite grafted with fluorination groups enhanced the homogeneity of the composite membrane prepared with Aquivion compared to composite membranes prepared with natural sepiolite. In addition to functionalization, a specific acidic post-treatment enhanced fuel cell performance. The acidic treatment was intended to remove some of the Fe cations in the sepiolite to prevent Aquivion degradation. Although this effect was not evident, this treatment removed some of the Al and Mg cations, resulting in a more amorphous structure of fluorinated sepiolite with increased porosity, roughness, and lumen. This significantly enhanced the proton diffusion in the composite membranes. Compared to commercially available membranes and membranes developed by other research groups, the Aquivion/fluorinated and post-treated sepiolite composite membranes (Aq/pSEP-F5) exhibited increased swelling behavior, water uptake, mechanical property, chemical stability, proton conduc-tivity, cell voltage, and maximum power density in the Membrane Electrode Assembly (MEA). Thus, they are highly advantageous and a promising alternative for the functioning of PEMFC at low relative humidity.

Keywords:
Sepiolite nanofiber (SEP)
Fluorination
Acidic pretreatment
Electrolyte membrane
Proton exchange membrane fuel cell (PEMFC)

1. Introduction

Fuel cells (FCs) are eco-friendly energy conversion systems that reduce carbon dioxide emissions. Hydrogen FCs, in particular, are regarded as a clean, renewable energy source that does not contribute to climate change. The fuel cells include various converters such as PEMFC, solid oxide fuel cell (SOFC), molten carbonate fuel cell (MCFC), alkaline fuel cell (AFC), and phosphoric acid fuel cell (PAFC). The description of FCs is shown in literature [1,2]. PEMFCs have been particularly beneficial in automotive applications owing to their advantages of low operating temperature, kick start-up, non-hazardous electrolytes, high power density and efficiency.

Proton-exchange membranes (PEMs) are composed of per-fluorosulfonic acid (PFSA) ionomers or hydrocarbon polymer electro-lytes. Among the PFSA ionomers, Nafion has been broadly selected as a reference because of its relatively great thermo-chemical properties, mechanical resistance, hydrophilicity, and performance in membrane electrode assemblies (MEAs). These beneficial properties originate from

* Corresponding author. Gwangju Clean Energy Research Center, Korea Institute of Energy Research (KIER), 270-25 Samso-ro, Gwangju, 61003, Republic of Korea.
** Corresponding author. MINES Paris, PSL University, Center for Processes, Renewable Energy and Energy Systems (PERSEE), CS 10207 rue Claude Daunesse, F-06904, Sophia Antipolis Cedex, France.
E-mail addresses: shwoo@kier.re.kr (S.H. Woo), christian.beauger@minesparis.psl.eu (C. Beauger).

the chain organization and chemically stable polytetrafluoroethylene (PTFE) of backbones and polyether side chains terminated with negatively charged groups of sulfonic acid (-SO_3H) [3,4]. However, Nafion electrolyte membranes show limitations when PEMFC are operated at low RH, causing dehydration responsible for the reduced proton conductivity. Aquivion, a PFSA ionomer, shows better properties from its higher glass transition temperature, larger crystallinity, lower equivalent weight with short side chain [5,6]. In particular, Aquivion exhibited better thermal stability than Nafion, allowing the membrane to operate at higher temperatures [7].

At high PEMFC operating temperatures, better kinetic reaction, easier heat, water management, and carbon monoxide (CO) tolerance are anticipated [8,9]. Because the PFSA phase alone is inadequate for higher temperatures and lower relative humidity, other inorganic fillers have been introduced as additives to develop new composite membranes. Incorporating inorganic fillers into a polymer matrix generally improves hydrophilicity, mechanical resistance, and, sometimes, proton conductivity. The inorganic fillers applied in composite membranes can be classified into three main categories: zeolites (e.g., ETS-10, NaA zeolite, umbite, mordenite, faujasite, analcime, ZrP-modified zeolite, b-zeolite, and H-type b-zeolite [10–15]), inorganic oxides (e.g., TiO_2, ZrO_2, ZrO_2/SO_4^{2-} , and SiO_2 [10,16–25]), and nanoclays (e.g., laponite, montmorillonite (MMT), sepiolite nanofiber (SEP), and halloysite nanotube (HNT) [10,11,26–33]).

Addition of nanoclays into the polymer phase has been specifically studied to reduce the limitations of thermomechanical stability and sensitivity to RH at high operating temperatures. Indeed, blending PFSA with nanoclay provides the benefit of maintaining moisture owing to its hygroscopicity. The resulting composite membranes showed improved proton conductivity at low RH [30,34–40]. Enhanced mechanical resistance [36,38,41–43], attributed to the better affinity between the fillers and the polymer phase, and sometimes reduced hydrogen crossover [44,45], can also originate from functionalized nanoclays homogeneously dispersed within the polymer matrix. Sepiolite, with its fibrous morphology commonly known as a needle-like structure [35,36] is a good candidate for enhancing the tensile strength of composite membranes through reinforcement. The authors previously reported the enhanced mechanical properties of Nafion and Aquivion composite membranes obtained after sepiolite introduction [35,36,39]. However, nanoclay aggregation can interfere with proton movement, and numerous research groups are still attempting to control the dispersion of nanofibers to improve PEMFC performance. To overcome this drawback, the surface functionalization of sepiolites, such as sulfonation [29, 36,46], or perfluorosulfonation [35], have been considered. Another critical factor in controlling the composite homogeneity is to set a short blending time of composite casting dispersions so that nanoclays do not clump together but disperse more easily.

Remarkable efforts have been achieved to improve the properties of sepiolite-blended composite membranes [39,40,47]. However, a study regarding physicochemical improvement resulting from the positive effect of an acidic treatment and the functionalization of sepiolite is lacking. Moreover, it is yet to be fully demonstrated that the strategy to fluorinate and post-treat the sepiolite improves conductivity and PEMFC performance under relative humidity below 30%. Thus, this study may be an interesting attempt to resolve the drawback of reduced fuel cell performance under dry operating conditions. Ultimately, it could be a promising strategy to improve the lifespan and reduce the manufacturing cost of hydrogen fuel cells by simplifying or removing the humidification system that controls relative humidity during operation.

In this study, we focus on the development of a novel sepiolite-incorporated Aquivion membrane that can be operated for PEMFC at a low RH below 30 °*C*. We demonstrated the improved properties of Aquivion composite membranes through sepiolite fluorination and pretreatment. The composite membrane (Aq/pSEP-F5) developed in this work displayed greater proton conductivity, proton diffusion coefficient, and proton concentration than the commercially available Nafion® HP or Gore Select® membranes, in addition to better mechanical properties than the virgin Aquivion membrane. Moreover, the chemical stability against the radical attack and fuel cell performance enhanced at 30% RH.

2. Experimental section

2.1. Materials

Sepiolite was provided by Tolsa. N-(3-triethoxysilylpropyl)perfluorooctanoamide (SPFOA) was purchased from ABCR. Ethanol, acetone, tetrahydrofuran (THF). All these products were used for functionalization without further purification.

Aquivion (24%, D83-24B) was purchased by Solvay. Sulfuric acid (H_2SO_4, 5 N), sodium hydroxide (NaOH, 98%) and hydrogen chloride (HCl, 0.1 N) were purchased from Alfa Aesar, Germany. Oxalic acid (0.45 M) were purchased from Fisher Scientific, UK. Sodium chloride (NaCl, 99.5%) and isopropanol (99.5%) were purchased from Acros Organics. Total ionic strength adjustment buffer solution (TISAB IV) and sodium fluoride (NaF) were purchased from Sigma Aldrich. Deionized (DI) water (18.2 MΩ cm) was supplied from ultrapure water plants (Smart2Pure, Thermo Scientific).

2.2. Sepiolite modification

Scheme 1 shows the fluoridation and post-treatment procedure for sepiolite nanofiber. Ten grams of sepiolite, 1 g of perfluorinated sepiolite (1.6×10^{-3} mol) with N-(3-triethoxysilylpropyl)-perfluorooctanoamide (SPFOA), and 100 mL of the water/ethanol (10/90 wt%) solution were added to a 250 mL flask fitted with a condenser. Subsequently, the heating mixture was stirred under reflux for 15 h. The centrifuge was operated at 5000 rpm to separate the liquid phase in the mixture. After then, it was washed several times with acetone and tetrahydrofuran. Finally, the functionalized clay nanofibers were dried under a vacuum prior to characterization. Sepiolite fluorination was achieved according to our previous protocol [39]. Natural and modified sepiolites were precipitated using membrane filters (pore size: 45 and 25 μm, Merck Millipore), and dried in an 80 °*C* oven at for 16 h.

To remove iron ions contained in sepiolite, the samples were treated using oxalic acid and hydrogen chloride solutions. One gram of sepiolite (pristine or modified) was stirred in 100 mL of 0.45 M oxalic acid ($C_2H_2O_4$) solution at 80 °*C* for 1.5 h. Nanoclays were then filtered using a membrane filter (0.4 μm of pore size, Merck Millipore) and washed using deionized (DI) water. Afterwards, the sepiolite was added to 100 mL of 0.001 M hydrochloric acid (HCl) and stirred at 80 °C for 2.5 h. Filtration and ultrasonication (HD2200, Bandelin) were repeated under specific conditions before washing and drying. Finally, the resulting clay nanoparticles were ground and stored in bottles. In terms of nomenclature, fluorinated sepiolite is labeled as SEP-F. Post-treated sepiolite samples are respectively labeled as pSEP or pSEP-F for pristine and fluorinated sepiolites.

2.3. Membrane preparation

The preparation of the membranes was done by following the previously published method [39]. Membranes (effective area: 13 × 13 cm^2) were prepared using dispersions by the casting and evaporation method. Aquivion dispersion (24%, D83-24B), virgin or modified sepiolite, and isopropanol were mixed to obtain a 5% Aquivion casting dispersion, resulting from evaporation in a 2, 5, or 10 wt% sepiolite-incorporated composite membrane, depending on the amount of sepiolite added (Table 1).

Different casting dispersions were mixed for 15 min at 80 rpm and then sonicated using ultrasonicator (Model: HD 2200, Bandelin, Germany) for 2 min at 60 W with 20% pulsation level. The membrane was

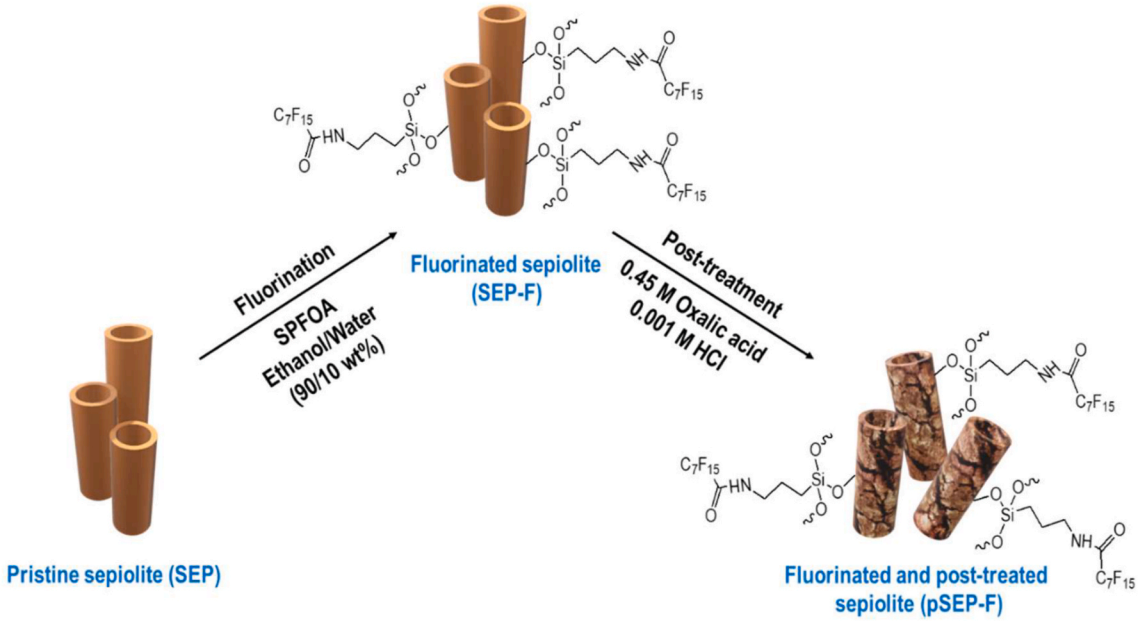

Scheme 1. Sepiolite nanofiber perfluorinated with SPFOA, and sepiolite post-treated with oxalic and hydrochloric acid.

Table 1
Chemical composition of pristine Aquivion and composite membranes containing SEP, SEP-F, pSEP and pSEP-F.

Membrane reference	Ionomer	Nanoclay reference/ content (wt%)	Modification of sepiolite	Post-treatment of sepiolite
Aquivion	Aquivion	–	–	–
Aq/SEP	Aquivion	SEP-10	Pristine	No
Aq/SEP-F	Aquivion	SEP-F-10	Fluorination	No
Aq/pSEP	Aquivion	pSEP-2/5/10	Pristine	Yes
Aq/pSEP-F	Aquivion	pSEP-F-2/5/10	Fluorination	Yes

Table 2
The S_{BET} and V_{total} according to the nanofiber samples.

Nanofiber samples	S_{BET} ($m^2\ g^{-1}$)	V_{total} ($cm^3\ g^{-1}$)
Pristine sepiolite (SEP)	155.47	0.44
Fluorinated sepiolite (SEP-F)	102.52	0.52
Post-treated sepiolite (pSEP)	143.05	0.67
Fluorinated and post-treated sepiolite (pSEP-F)	193.01	0.73

prepared by pouring the casting dispersion into the mold and then heating it at 80 °*C* for 18 h, followed by 170 °*C* for 2 h. Finally, the prepared membranes were treated using 0.5 M sulfonic acid (H_2SO_4) and rinsed with deionized water for 1 h at 100 °*C*.

Regarding the nomenclature, SEP and SEP-F denominate virgin sepiolite and fluorinated sepiolite, respectively. Prefix p was added to the post-treated sepiolite. 2, 5, and 10 represent the sepiolite loading in wt%.

Gore Select® and Nafion® HP were selected as reference membranes to compare the characteristics of the prepared composite membranes.

3. Analytical methods

3.1. ATR-FTIR

The functionalization of the sepiolite surface was characterized by FTIR spectroscopy using an IFS 66 apparatus from Bruker. Spectra from 400 to 4000 cm^{-1} were obtained by accumulating 32 scans at a resolution of 4 cm^{-1}.

3.2. TGA

TGA was conducted to study the surface fluorination and acidic treatment of sepiolites. Analyses were performed using a PerkinElmer Pyris-1 instrument. An isothermal step (10 min, 110 °C) was performed to remove the physisorbed water, and then the samples were heated to 900 °C at a heating rate of 10 °C/min. Analyses were performed with samples of approximately 10 mg under a nitrogen at a flow rate of 20 mL/min.

3.3. XRD

The X-ray diffraction (XRD) patterns of the post-treated and non-treated sepiolites were analyzed using Cu-Kα radiation (λ = 1.5406 Å) using an X-ray diffractometer (X'Pert-Pro, Philips). The diffractometer was operated at 30 and 45 kV. The data were collected in steps of 0.08° from 4° to 60° in the 2-θ mode with a pixel step.

3.4. FE-SEM and EDS

Cross-sectional images of the prepared membranes were obtained by FE-SEM (FEI XL30, Philips) at 2000 × magnification. The Si/F (atomic ratio in %) for the upper, middle, and bottom locations of the membrane cross-section was calculated using EDS to analyze the dispersion of clay nanofibers inside the polymer phase. The Fe/Si, Mg/Si, and Al/Si atomic ratios (at.%) were also analyzed for SEP, pSEP, SEP-F, and pSEP-F clay nanofibers.

3.5. BET

Sepiolite nanofibers were degassed at 120 °C for 24 h under a static vacuum before the adsorption measurements. The specific surface area was determined from the N_2 adsorption isotherms in the relative pressure range 0.05–0.20, using the Brunauer–Emmett–Teller (BET) method (BEL MINI, BEL Japan Inc.). The total pore volume (V_{total}) was estimated using the amount of gas adsorbed at a relative pressure of $P/P_0 = 0.99$. Micropore volumes were calculated from the corresponding isotherms using the t-plot method.

3.6. TEM

TEM samples were prepared using the conventional drop-casting method. The samples were investigated by analytical TEM (JEM-ARM200F NEOARM, JEOL Ltd.) at 200 kV and energy-dispersive X-ray spectrometry (EDS) (JED-2300T, JEOL Ltd.). The elemental distributions of SEP-F and pSEP-F were determined by STEM-EDS.

4. Membrane thickness

Square wet membranes (preliminarily soaked in DI water for one day) were cut into nine equal squares. The thickness of three of them, selected on the diagonal, was measured at three different places per piece of the membrane using a micrometer (Mitutoyo 293–344, Japan). Subsequently, the average thickness was calculated based on nine data points per membrane. The thickness of the dry membranes was also measured through FE-SEM cross-sectional observation and averaged using data from three measurements.

4.1. Water uptake

The weight difference between the wet and dried membranes was measured to calculate the water uptake. The membranes were then immersed in DI water at room temperature. For dehydration, the membranes were dried in an oven set at 80 °*C* for 18 h. The water uptake of the prepared membranes was calculated using the following equation:

$$WU_{wt}\ (\%) = \frac{W_w - W_d}{W_d} \times 100 \tag{1}$$

Where W_w and W_d are the weights of the wet and dried membranes, respectively.

4.2. Swelling ratio

Two types of membrane swelling were calculated based on the evolution of the membrane thickness between 1) dry and wet conditions at room temperature and 2) room temperature and boiling temperature after 2 h of immersion. The thickness of all membranes was averaged based on data measured at three different locations, and swelling was calculated using the following equations:

$$S_{th\_1}(\%) = \frac{th_{wet\_rt} - th_{dry\_rt}}{th_{dry\_rt}} \times 100 \tag{2}$$

$$S_{th\_2}(\%) = \frac{th_{wet\_bt} - th_{wet\_rt}}{th_{wet\_rt}} \times 100 \tag{3}$$

where th_{wet_rt} and th_{wet_bt} are the thicknesses of the wet membranes after immersion 2 h in water at room temperature and 100 °*C*, respectively. th_{dry_rt} represents the thickness of the dried membrane.

4.3. IEC

IEC was obtained by titration. The membranes were fully immersed for 1 d in a 2 N sodium chloride (NaCl) solution (40 mL) for Na^+ ions to replace H^+ ions in the membrane. The protons were then titrated using a 0.005 N sodium hydroxide (NaOH) solution. IEC was calculated using the following equation:

$$IEC\ (meq\ /\ g) = \frac{C_{NaOH} \times V_{NaOH}}{W_d} \tag{4}$$

where C_{NaOH} and V_{NaOH} represent the concentration and volume of the NaOH, respectively. W_d represents the weight of the dried membranes.

4.4. Chemical stability (modified Fenton test)

The membranes can be chemically degraded in the presence of iron during fuel cell operation. The fluoride concentration in the water increases while iron attacks the C-F bonds of Aquivion. Thus, the chemical stability can be assessed by fluoride analysis. One piece of each membrane was immersed in a 200 mL 4.4 M H_2O_2/1.25 mM H_2SO_4 solution to reach 0.16 wt%, under stirring at 100 rpm and 70 °*C*. The membrane was kept in the solution for 4, 17, 48, 72, and 96 h. Total-ionic strength adjustment buffer (TISAB IV) was then mixed before 0.001 N NaF solution was added as the standard for analysis. Subsequently, the fluoride concentration in the solution was measured with a specific electrode (781 pH/Ion meter, Metrohm AG, Switzerland). A blank test of the solution was performed before analysis.

4.5. DMA

The viscoelastic properties of the membranes were characterized using dynamic mechanical analysis (DMA50, Metravib, Acoem) under shear jaws for the film test configuration. The dimensions of the samples were set to 30 mm in length and 10 mm in height, and the thickness of the membrane was between 30 and 50 μm. The results were obtained using DYNATEST software. The temperature was scanned between 50 and 200 °C at a heating rate of 1 °C/min. It was previously verified that the deformation (3 μm) is in the linear domain. The frequency was set at 1 Hz.

4.6. Electrochemical impedance spectroscopy

The resistance of the membranes was accurately measured using electrochemical impedance spectroscopy (EIS; Bio-Logic Scientific Instruments, France). One piece of the membrane was placed between the two electrodes of a homemade cell. The operating conditions were set at 50 °C, 70 °C, or 90 °C, and relative humidity (RH) of 25%, 50%, 75%, or 90%. The frequency range and amplitude were set to 1 mHz–1 kHz and ±20 mV, respectively. The membrane resistances (Ω) were averaged from the data from 50 scans. The proton conductivity (S/cm) was then obtained for all membranes by the following equation:

$$\sigma = \left(\frac{l}{R.S}\right) \tag{5}$$

where σ is the proton conductivity (S/cm) and R and l represent the resistance (ohm) and thickness (cm) of the membrane, respectively. S represents the contact surface with the electrodes (cm^2).

4.7. MEA preparation

Sono-Tek ExactaCoat ultrasonic spray-coating system was used to deposit catalyst layers on both sides of the membranes, fixed on a vacuum plate heated to 80 °*C*, and prepare 50 cm^2 active surface area catalyst coated membranes (CCMs).

The catalyst (TEC10E40E) loadings for the anode and cathode were 0.26 ± 0.08 mg Pt/cm^2 and 0.50 ± 0.06 mg Pt/cm^2, respectively. Subgaskets (PET) and gas diffusion layers (Freudenberg H23C6) were hot-pressed (15 h at 50 kg/cm^2, Carver 30-12H Press) on both sides of the CCM respectively at 170 and 140 °*C* for Aquivion-based and Nafion HP membranes.

4.8. Fuel cell performance

The MEAs were tested on a single-cell fuel-cell test bench. Polarization curves (U = f(j)) were obtained at 80 °C and at 30% RH under dry condition and 100% RH under wet condition. The MEA resistance was measured using impedance spectroscopy and assimilated to the high-

frequency impedance value for its imaginary part equal to zero. The target relative humidity was set and regulated by the mass flow controllers (MFCs) installed on a single-cell fuel-cell bench and the use of home-made software.

Regarding hydrogen crossover, the cell was purged with hydrogen on the anode side and with nitrogen on the cathode side. A three-electrode set-up was used where the anode serves as reference and counter electrode and the cathode acted as the working electrode. The voltage was scanned from 0.05V to 0.55V at 5 mV/s.

5. Results and discussion

5.1. Sepiolite characterization

Fig. 1a shows the thermal gravimetric analysis (TGA) curves of pristine (SEP) and fluorinated sepiolites (SEP-F). Fluorinated sepiolites showed increased weight losses (Fig. 1a) compared to pristine sepiolites, which can be ascribed to the decomposition of the grafted fluorinated groups, confirming our previous work [39]. Fluorinated sepiolites were found to have 1.4 wt% increased weight loss compared to pristine sepiolites due to the decomposition of the grafted fluorinated groups. In addition, non-post-treated sepiolite showed a higher rate of decrease from 240 °C than post-treated sepiolite, regardless of fluorination, as aluminum and magnesium hydroxyl groups begin to decompose at 240 °C and 330 °C, respectively. Interestingly, the post-treated sepiolite exhibited the highest residue 91.7 wt% among the clay nanofibers tested, which is approximately 1.2 wt% gap between post-treated and non-treated sepiolites. Further experiments are required to determine which modifications to the chemical structure led to these outcomes.

For the Fourier transform infrared (FTIR) analysis, similar spectra were obtained for the pristine and fluorinated sepiolite nanofibers (Fig. 1b) [39,48]. The Mg-OH and inside Mg-OH stretching vibrations appeared at 3548 and 3670 cm^{-1}, respectively. The bands at 640 and 684 cm^{-1} are attributed to the O-H bond vibration of Mg_3OH. The band at 420 cm^{-1} is due to octahedral-tetrahedral bonds (Si-O-Mg). The bands at 973, 1081 (shoulder), and 1243 cm^{-1} respond to the vibration of Si-O bonds within silica tetrahedra. The bands at 430, 990 cm^{-1} are attributed to Si-O-Si groups. The band at 1658 cm^{-1} is originated from the zeolitic water of the sepiolite nanofibers. However, the fluorinated sepiolite nanofibers showed few differences owing to the grafted agent compared with the pristine sepiolite nanofiber. As described in a previous study, a signal of the C-F bonds of the perfluorinated part was observed at 1240 cm^{-1} [39]. We also observed a band at 1370 cm^{-1}, which is characteristic of the C-H stretching vibration of the alkyl part of the grafted organic agents (Fig. 2b).

Sepiolite can be sensitive to acid treatment. Thus, it is necessary to check the integrity of the sepiolite structure after post-treatment with oxalic acid and hydrogen chloride. Complementary FTIR analysis (Fig. 2c and d) revealed that the intensities of the Mg-OH (640, 684, 3548, and 3670 cm^{-1}), Si-O-Mg (420 cm^{-1}), Si-O (973 and 1243 cm^{-1}) and Si-O-Si (430 and 990 cm^{-1}) groups decreased after post-treatment (pSEP and pSEP-F vs. SEP and SEP-F). The structure of sepiolite nanofibers is thus sensitive to acid attack, and its intensity was reduced compared to non-post-treated SEP and SEP-F nanofibers, which is in good agreement with the results reported in the literature [48]. This indicates that sepiolites probably changed to an amorphous structure post-treatment (Fig. 1c and d).

The structure of sepiolite post-treated alone or fluorinated together was observed to be mainly amorphous in Fig. 1e. As reported for palygorskite [49], such cation leaching may lead to the structural modification analyzed using X-ray diffraction (XRD). This results in a fraction of octahedral voids at the edges of channels composed of silanol groups

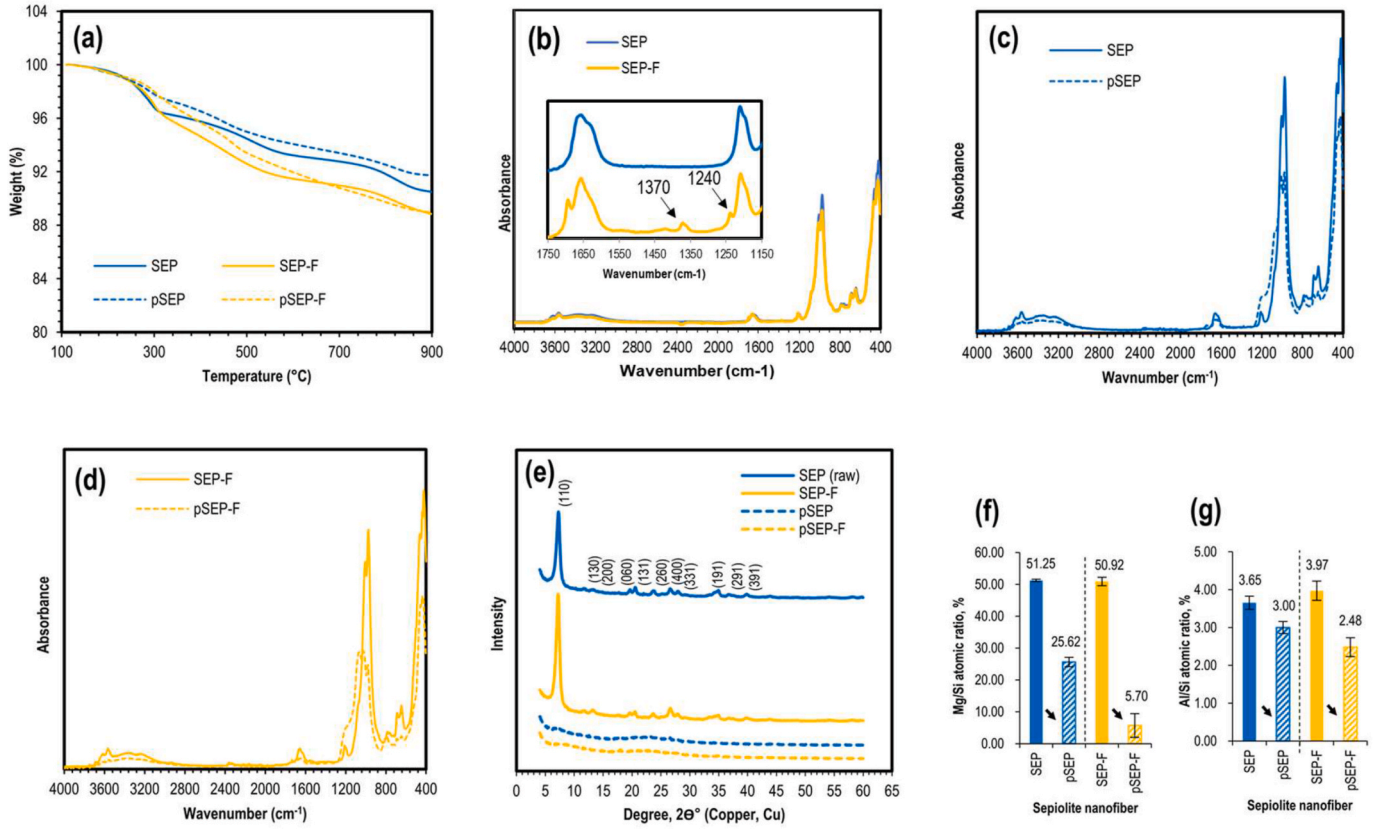

Fig. 1. Analytical results of (a) TGA curves and (b, c, d) ATR-FTIR spectra for SEP (blue), SEP-F (yellow), pSEP (blue dashed) and pSEP-F (yellow dotted) nanofibers used as in-membrane filler. (e) XRD spectral data of sepiolite after treatment: SEP (blue), SEP-F (yellow), pSEP (blue dotted), and pSEP-F (yellow dotted) nanofibers used as in-membrane fillers. Comparison of (f) Mg/Si and (g) Al/Si atomic ratios (%) for SEP, pSEP, SEP-F, and pSEP-F nanofibers used as in-membrane fillers.

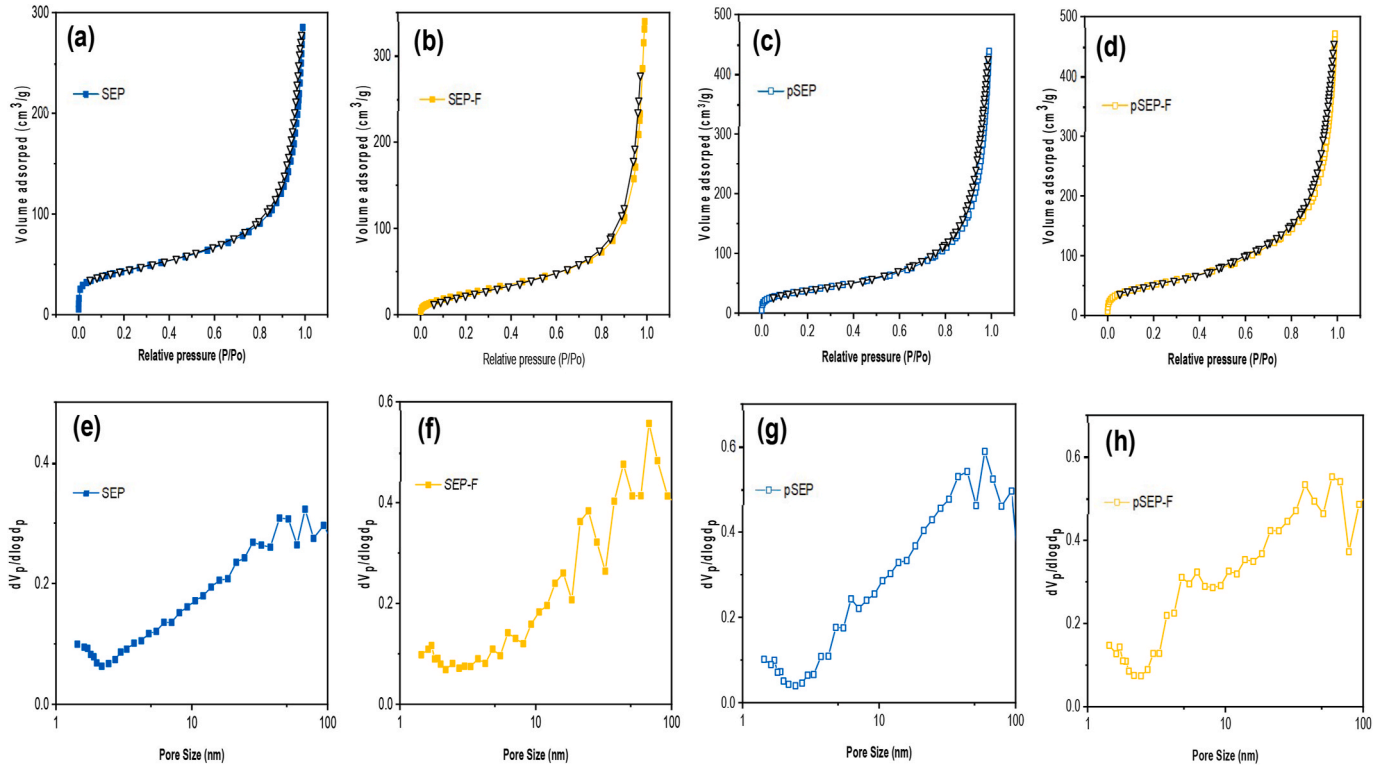

Fig. 2. Data for (a to d) the nitrogen sorption isotherms measured at 77 K (−196.15 °C), and (e to h) BJH plot in SEP, SEP-F, pSEP, pSEP-F nanofibers. The specific surface area (S_{BET}) and total pore volumes (V_{total}) of sepiolite nanofibers are listed in Table 2.

(Si-OH) and, consequently, a modification of the surface area [50–52]. Leaching led to the structural modification, allowing no further crystallinity. The results of energy dispersive X-ray spectroscopy (EDS) implied that the relative concentrations of cations such as Mg^{2+} as well as Al^{3+} present inside the sepiolite were reduced by the acid treatment (Fig. 1f-g).

The pore sizes of the sepiolite nanofibers ranged from 11 to 20 nm, whereas the Barrett, Joyner, and Halenda (BJH) plot of the sepiolites was approximately 2–100 nm. The total pore volumes of SEP, SEP-F, pSEP, and pSEP-F were 0.44, 0.52, 0.67, and 0.73 cm^3/g, respectively, as determined by the method of the Brunauer–Emmett–Teller (BET) (Fig. 2). A specific surface area of sepiolites between 102 and 193 m^2/g was observed, especially for pSEP-F, which showed the largest specific surface area among the sepiolite nanofibers tested. The highest total pore volumes were also obtained for pSEP and pSEP-F compared to SEP and SEP-F. This might be attributed to the reduced Mg and Al dissolved by the acidic post-treatment (Fig. 1f and g), which ultimately developed pores in the sepiolite samples, thereby increasing their specific surface area and pore volume. Indeed, it was visually observed using transmission electron microscopy (TEM) to confirm whether the fluorinated and post-treated sepiolite pores were formed. The outer pore size change, enlarged inner diameter (lumen), surface roughness, and surface fluoride ratio of the fluorinated and post-treated sepiolite observed using TEM are described in in more detail in the section Impact of fluorination and post-treatment on sepiolite.

5.2. *Iron content in sepiolite and chemical resistance of membranes*

The PFSA membrane is prone to exposure to free radical species during fuel-cell operation. OH • and OH_2 • radicals with strong oxidative properties chemically attack the C-F bonds, ultimately reducing the cell performance efficiency [53]. H_2O_2 can be produced at the cathode of the MEA via the two-electron reduction of oxygen. It then reacts with the Fe^{2+} ion to generate free radical species (i.e., HO· and HO_2·) [10,54–56].

Sepiolite nanofibers may contain iron ions that can chemically degrade composite membranes in the presence of hydrogen peroxide. Oxalic acid and hydrogen chloride were used and evaluated as means of leaching iron from sepiolite. To verify whether sepiolite-blended membranes are chemically stable, we used a "modified" Fenton test. The composite membranes containing sepiolite as the hypothesized source of ferric (II) ions were immersed in a H_2O_2/H_2SO_4 solution. The fluoride concentration generated by chemical degradation was followed by a specific electrode of ion meter. It should be noted here that post-treated sepiolites incorporated in composite membranes were obtained using oxalic acid and hydrogen chloride treatment. The modified Fenton test was conducted via H_2O_2/H_2SO_4 treatment of composite membranes.

Fig. 3 displays the fluoride ion concentration for all the membranes analyzed at various reaction times between 4 and 96 h. It is noteworthy that the post-treatment was efficient with iron leaching. The amount of Fe with respect to that of Si, being decreased by 50%–80% respectively for pristine and fluorinated sepiolite (Fig. 3b). The evolution of the fluorine ion concentration with time was comparable for all the membranes tested: the longer the reaction time in the H_2O_2/H_2SO_4 solution, the higher the fluoride concentration. This value is slightly greater for the reference membrane and approximately double for the pristine Aquivion membrane.

Notably, the presence of sepiolite did not amplify membrane degradation. When attacked by free radical species, the concentration of fluoride ions generated by our ion exchange membranes was significantly lower than that of the reference membranes. No significant differences were found between the composite membranes. Therefore, it can be suggested that fluorination and post-treatment of sepiolite are neither detrimental nor advantageous to the chemical resistant of composite membranes.

Rio et al. reported that 20 different sepiolites from a variety of sources, including Madrid, Toledo, Zaragoza, and California deposits, did not contain ferric (II) ions [57]. This finding was consistent with our observations. In this study, the sepiolite used to develop the membranes

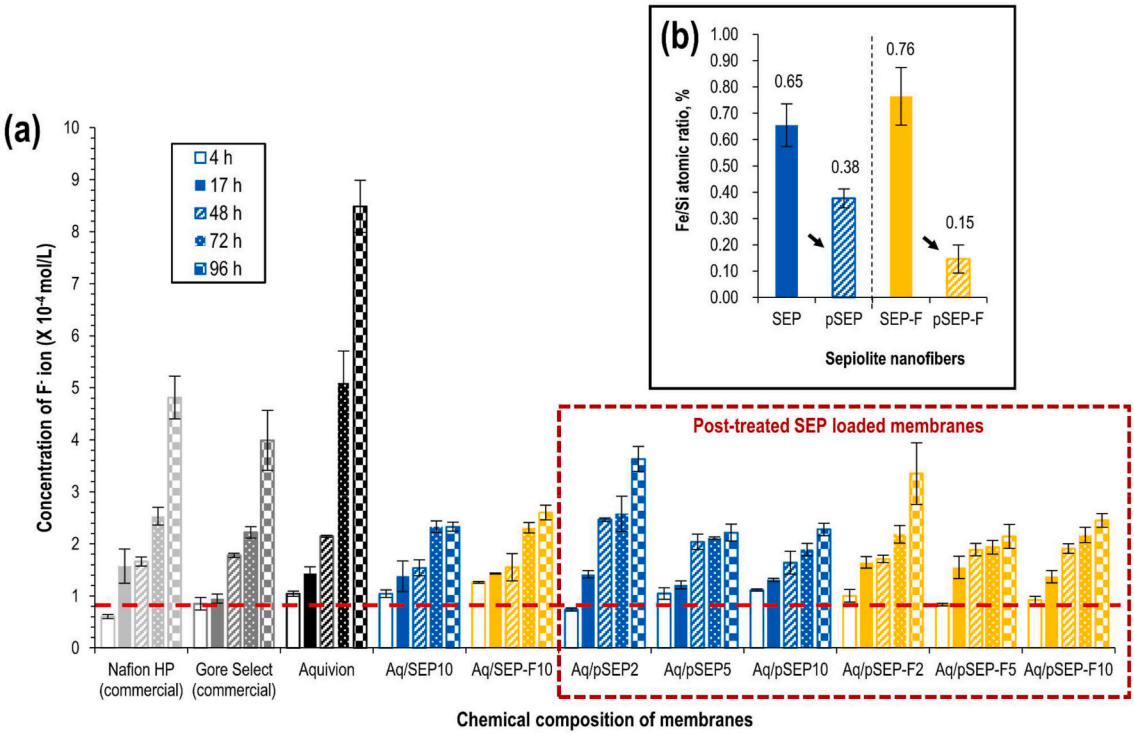

Fig. 3. Data analyzing the chemical resistance (i.e., fluoride ion concentration) of membranes by immersion in H_2O_2/H_2SO_4. The red dotted line indicates the fluorine concentration of 4.4 M H_2O_2/1.25 mM H_2SO_4 electrolyte (blank test): $0.82 \times 10^{-4} \pm 0.08 \times 10^{-4}$ mol L^{-1}. Comparison of (b) the iron content in sepiolite used for preparing composite membranes before and after post-treatment with oxalic acid and hydrochloric acid.

was a Tolsa product, which was mined in Madrid and did not contain a large amount of ferric (II) ions. The observed relative stability of the membranes indicated that the ferrous (III) ions from sepiolite were not reduced to the ferric (II) ions. Notably, iron ions can be converted between Fe^{2+} and Fe^{3+} in the presence of free radicals, as reported in the literature [58,59].

5.3. Homogeneity of composite membranes

Fig. 4 displays cross-sectional images obtained using field emission scanning electron microscope (FE-SEM) of the various membranes prepared according to the experimental section. The chemical composition was analyzed using EDS to obtain insights on the repartition of sepiolite nanoclays at center and edges of the membrane cross-section.

To this end, silicon and fluor of Aquivion were analyzed explicitly as representatives of sepiolite and Aquivion, respectively. Subsequently, the Si/F atomic ratio was considered an indicator of homogeneity. A constant Si/F value obtained from nanoclay was considered uniformly distributed across the membrane; otherwise, nanoclay aggregates were suspected.

Composite membranes blended with pure sepiolite and Aquivion show inhomogeneity (Aq/SEP10, Fig. 5d). The significant difference in the Si/F atomic ratio obtained from EDS analysis of the composite membrane (Fig. 4l) was in good agreement with the presence of bulky aggregates, as shown in Fig. 4d.

Sepiolites grafted with fluorine groups (SEP-F10, pSEP-F10, pSEP-F5, and pSEP-F2) improved the homogeneity of the composite membranes. Fewer aggregates were observed in the corresponding cross-sectional images (Fig. 4h-k). Smaller differences in Si/F values were also observed, as shown in Fig. 4l. Such fluorination was expected to improve the affinity between Aquivion and the grafted sepiolite. More specifically, the fluorine groups of sepiolite functionalized with N-(3-triethoxysilylpropyl)-perfluorooctanoamide resulted in better interaction with the hydrophobic domain C-F of the Aquivion matrix, leading to better compatibility and homogeneity [35].

Post-treatment with oxalic and hydrochloric acid was used to iron ions from sepiolite to improve the chemical stability of the composite membranes. It also seems to prevent the aggregation of sepiolite (Fig. 4e-g and Fig. 4l) [52,60–62], with respect to the various conditions of sepiolite (2, 5, or 10 wt%), be fluorinated. Therefore, very few agglomerates can be observed, as can be seen in Fig. 4e-g. The best homogeneity was obtained for fluorinated and post-treated sepiolite among the membranes prepared because no visible agglomerates could be observed. In addition, constant Si/F values could be estimated across the membranes. Moreover, EDS images obtained from F (red) and Si (green) elemental color mapping analysis of the Aq/pSEP-F membranes, which were the most dispersed of the observed membranes, are shown in Fig. S2. It was observed that the 2% and 5% pSEP-F nanoclays were largely well dispersed within the Aquivion matrix, but partially aggregated. The 2% loading in membrane appears slightly more homogeneous than the 5% loading.

5.4. Membrane thickness

The thinner the membrane, the smaller the ohmic resistance, sometimes at the expense of a larger hydrogen crossover [63]. State-of-the-art membranes are now less than 20 μm thick. Hence, the targeted thickness for the membranes prepared in this study was 20 μm under dry state, similar to that of the commercially available Gore Select® or Nafion HP® membranes selected as references. Fig. 5a shows the thickness of the membranes measured in the dry state using FE-SEM. Thicknesses in the wet state were also measured using a micrometer after immersion in DI water at room temperature or boiling water. The results (Fig. 5d) are discussed later, along with the water uptake and swelling.

In the dry state, the thickness of the prepared membranes was very close to that of the target, between 19 and 28 μm. The incorporation of fluorinated sepiolite did not affect the thickness, which remained at approximately 25 μm. The post-treatment of sepiolite resulted in a

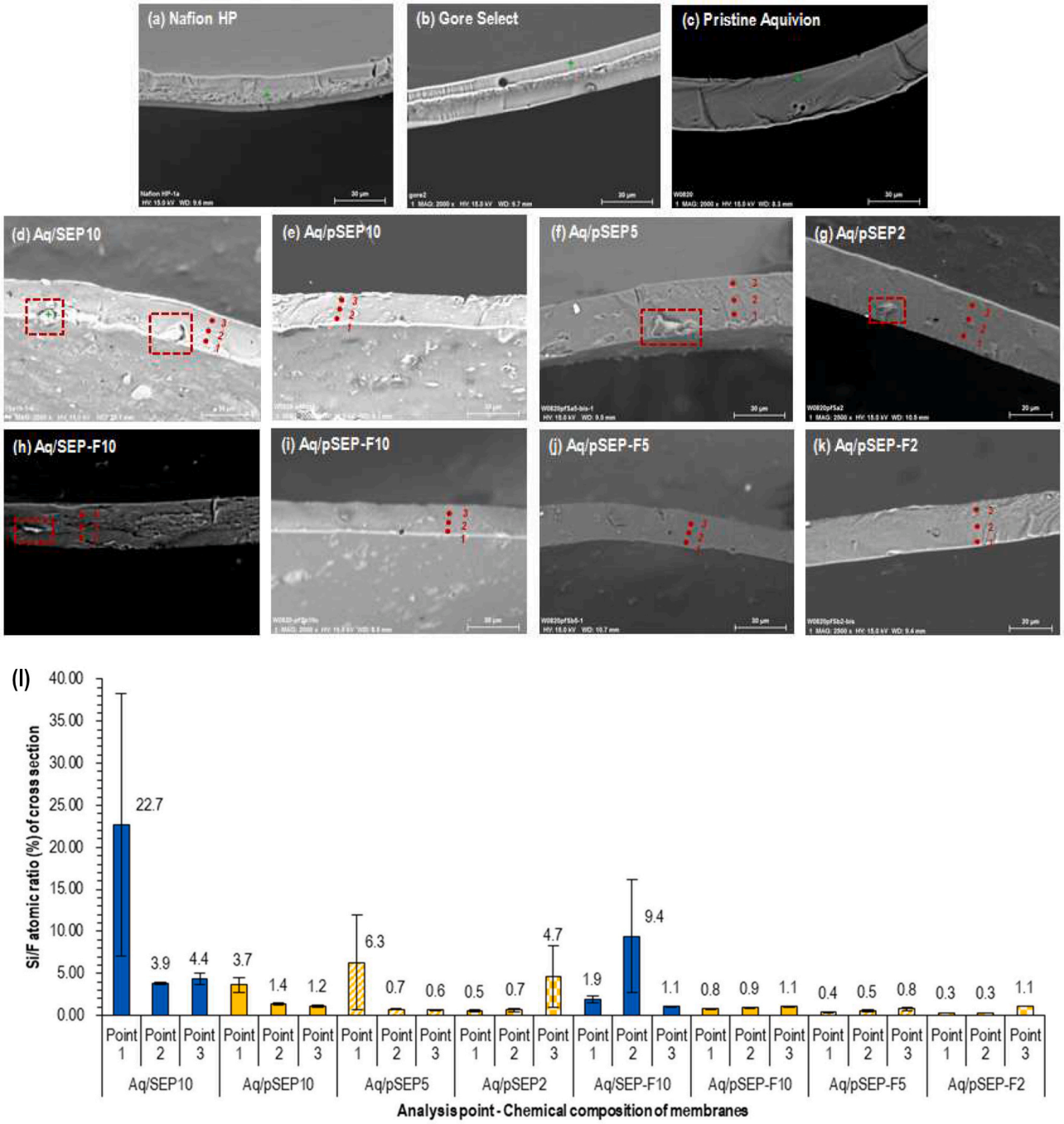

Fig. 4. Images observed using FE-SEM for (a-b) commercially available membranes, (c) pristine Aquivion membrane, and (d-k) composite membranes. Partly reproduced with permission from Elsevier Ltd [39]. Resulting data on (l) Si/F atomic ratio (%) analyzed using EDS in a membrane cross-section. Blue and yellow bars indicate non-post-treated sepiolites and post-treated sepiolites, respectively. The different patterns represent different additive contents.

relatively small modification of the composite membrane thickness, without any clear trend, which may reach a maximum of 5 wt%.

5.5. Ion exchange capacity (IEC)

IEC is an important property that represents the total capacity of functional groups. It strongly affects the transport of protons across membranes, particularly Grotthuss-type transfer [63]. The IEC values for the composite membranes differed slightly from those of pristine Aquivion and commercially available membranes, as shown in Fig. 5b. To be specific, the IEC for pristine Aquivion was about 1.02 meq/g, whereas composite membranes containing sepiolite (i.e., SEP or SEP-F) was measured to 1.08–1.20 meq/g, depending on the level of fluorination. The Nafion HP membrane exhibited a similar IEC of 1.08 meq/g to the pristine Aquivion membrane, but a slightly lower IEC (0.98 meq/g) to the Gore Select membrane. Among the membranes prepared with post-treated sepiolites (i.e., pSEP, pSEP-F), the IEC seems to reach a maximum for 5 wt%. These results showed a similar trend to the water uptake data with the exception of the 10 wt% sepiolite-contained membrane. This error value could be caused by temperature differences or water uptake values in the IEC analysis.

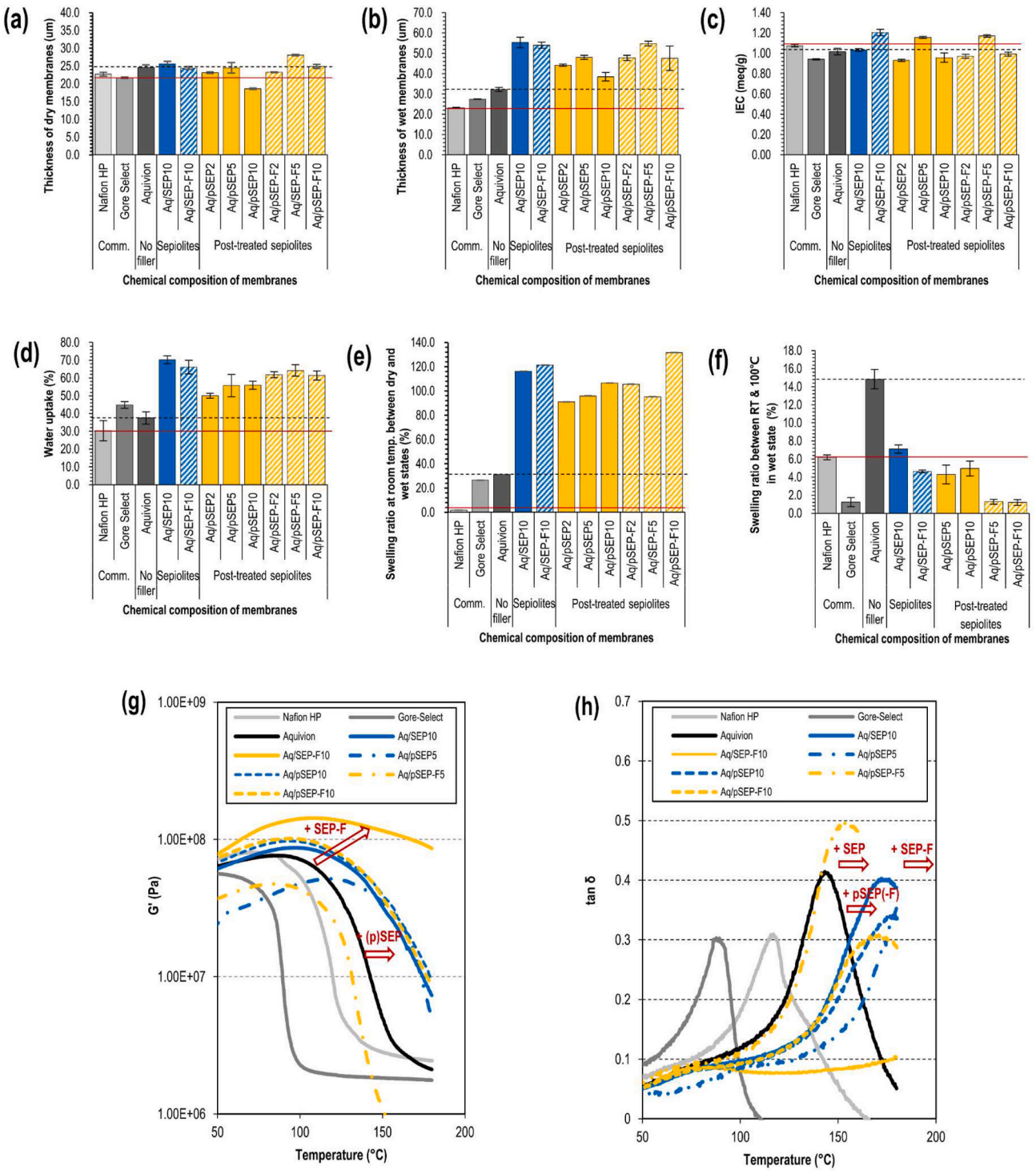

Fig. 5. Results on (a) dry thickness, (b) hydrated thickness, (c) IEC, (d) water uptake, (e) swelling at room temperature between dry and wet states, and (f) swelling between room temperature and 100 °*C* in the wet state regarding Nafion HP, Gore Select, virgin Aquivion and Aquivion reinfoced membranes incorporated with various sepiolites. Gray bars indicate reference membranes. Blue and yellow bars indicate post-treated sepiolites and non-treated sepiolites, respectively. The diagonal line patterns represent fluorinated sepiolites. DMA results: (g) G′ and (h) tan delta regarding Nafion HP, Gore Select, virgin Aquivion, and Aquivion reinforced membranes incorporated with sepiolites, fluorinated only, or post-treated together.

5.6. Water uptake and swelling

Water molecules are necessary for proton transport in proton exchange membranes according to the Grotthuss mechanism, so-called hopping mechanism, or vehicle mechanisms [64–66]. Hence, water uptake is another critical property to characterize.

As can be seen in Fig. 5d, the addition of sepiolite to Aquivion, whether modified or not, results in a remarkable increase in water uptake compared to Nafion® HP, Gore Select®, and virgin Aquivion membranes. Water uptake of about 80–90% more was achieved after incorporating 10 wt% of sepiolite, pristine or fluorinated form, due to its high hygroscopic nature. It seems that post-treatment is responsible for a slight decrease in water uptake, which, however, remains significantly large. From the results obtained with post-treated sepiolite, it is clear

that the larger the amount of sepiolite, the larger the water uptake.

A larger water uptake is beneficial for PEMFC operation at low relative humidity. However, it generally leads to larger swelling, which may be detrimental as it can affect fuel cell performance during its operation. Here, two types of swelling have been considered: i) Room temperature between dry and wet states to characterize the impact of water uptake on the thickness and ii) Temperature between room temperature and "high" temperature (after immersion in boiling water) to report the evolution of the membrane thickness during operation in a PEMFC (i.e., 80 °C or above).

First, it is clear from Fig. 5d that water uptake has a marked impact on the membrane thickness.

In general, the membrane thickness increases with the amount of sepiolite added to the Aquivion polymer and is above 45 μm. The membrane thickness also varies with oxalic and hydrochloric acid post-treatment.

The membrane incorporating pristine sepiolite (SEP10, 10 wt%) had a thickness of 55.3 ± 2.5 μm, which is thicker than the pristine Aquivion membrane.

Fluorinated sepiolite did not affect the composite membrane thickness (Aq/SEP-F10: 54 ± 1.6 μm).

The post-treatment of sepiolite in oxalic acid and hydrogen chloride results in thinner composite membranes 38.4 ± 2.1 to 48.0 ± 1.0 μm for pristine sepiolite and 47.6 ± 5.9 to 54.8 ± 1.1 μm for fluorinated one, depending on the amount incorporated in Aquivion, the thickest being obtained for 5 wt%.

Such an impact of the water uptake on the membrane thickness transfers directly to the swelling between dry and wet states at room temperature (Fig. 5e).

For all composite membranes, significantly higher swelling was obtained compared to the pristine Aquivion membrane: about +120% for composite membranes prepared with 10 wt% of pristine or fluorinated sepiolite, between +90 and 130% for post-treated sepiolite, depending on the composite composition.

The effect of temperature on the swelling of hydrated membranes showed interesting results for the composite membranes. As represented in Fig. 5f, Nafion® HP and Gore Select®, which are reinforced membranes, had rather low swells of 6% and 1.2%, respectively. A much higher value of approximately 15% was obtained for pristine Aquivion membrane, not reinforced.

The incorporation of sepiolite, whether or not functionalized and post-treated, led to a very significant drop in the swollen thickness of the composite membranes compared to pure Aquivion: 50% less swelling with 10 wt% sepiolite, even more was observed when the sepiolite was fluorinated or post-treated. The lowest swelling (1%) was observed for fluorinated and post-treated sepiolite. This behavior can be attributed to a reinforcement of the acicular nature of sepiolite nanofibers, as discussed in our previous study on Nafion® composite membranes [35,36].

Concerning fluorination, the presence of $-C_7F_{15}$ groups in the adapted sepiolite (SEP-F10) probably led to enhancement of the mechanical property due to the needle-like sepiolite by improving the nanophase distribution and the rapport between the filler and the hydrophobic domains of the Aquivion matrix [35,66].

Fluorination of the sepiolite and post-treatment with hydrogen chloride and oxalic acid caused a significant decline in swollen thickness, which was reached to the similar value as that observed in the Gore-Select reinforced membrane. This synergistic impact was in accordance with the influence of observed homogeneity of the composite membrane. The most homogenous membranes were obtained with the post-treated and fluorinated sepiolite (pSEP-F10 and pSEP-F5, Fig. 4i).

5.7. Dynamic mechanical analysis (DMA)

In terms of the mechanical properties of the membrane, a comparison of the different trends using DMA in shear mode is shown in Fig. 5gh.

The drop in G' appeared at higher temperatures for Aquivion compared to Nafion® HP and Gore Select (Fig. 5g), revealing a higher stiffness. Consequently, Aquivion exhibited a high glass transition temperature (T_g) of 140 °C (Fig. 5h).

Performance was improved by adding 10 wt% sepiolite nanofibers to Aquivion (Aq/SEP-10). The composite membrane was stiffer with a Tg shift towards 170 °C compared to the pure Aquivion® membrane. The fluorinated sepiolite led to a higher stiffness, and the T_g of the composite membrane (Aq/SEP-F10) appeared to shift to a much higher temperature (out of the available temperature range).

On the other hand, sepiolite pretreatment had no additional effect on mechanical strength: the composite membranes displayed similar stiffness and T_g as comparing to untreated sepiolite-incorporated membranes, despite functionalization. However, the composite membrane's glass transition temperature (around 160–170 °C) is stable in the thermo-mechanical property when the fuel cell is operated at intermediate temperatures.

5.8. Proton conductivity

The hydrogen ion conductivity for membrane samples was estimated from electrochemical impedance spectroscopy data recorded under various temperatures (i.e., 50 °C, 70 °C, and 90 °C) and relative humidity (i.e., 25%, 50%, 75%, and 90%). Because the membranes were automatically hydrated, the proton conductivity was calculated considering the thickness in the wet state. According to Fig. 7, proton conductivities calculated for different kinds of Aquivions were similar to values at 25% RH or 90% RH on 90 °C, as reported in literature [67–69].

As a general rule, all membranes become more protonically conductive at higher temperatures and relative humidity (Fig. 6 and S1). As expected, the effect of temperature was much more pronounced than that of relative humidity.

Based on Fig. 6, regardless of the temperature and RH, the proton conductivities of the composite membranes can be categorized as follows: Aq/SEP10 < Aq/pSEP10 ≤ Aq/pSEP5 < Aq/SEP-F10 < Aq/pSEP-F10 < Aq/pSEP-F5. It appears from this classification that both fluorination and post-treatment improve membrane proton conductivity, which is more effective than post-treatment and mixing, resulting in the highest conductivity (Aq/pSEP-F10 > Aq/SEP-F10 > Aq/pSEP10 > Aq/SEP10). Moreover, for 2, 5, and 10 wt%, adding 5 wt% sepiolite to Aquivion gave the best results (Aq/pSEP-F5 > Aq/pSEP-F2 > Aq/pSEP-F10 and Aq/pSEP5 ≥ Aq/pSEP10).

The hydrogen ion conductivity of the virgin Aquivion membrane prepared in this study (0.115 S/cm at 90 °C and 90% RH) was very similar to that reported in the literature under same conditions [67,68]. It stands between that of the composites incorporating non-fluorinated sepiolite and fluorinated ones, whether post-treated or not.

For the membrane incorporating pure sepiolite (SEP10) into Aquivion, a reduced proton conductivity was observed compared to pristine Aquivion and Nafion® HP. This phenomenon may be due to sepiolite aggregation and possible blockage of ion channels, which hinder ion transport inside the composite membrane.

Fluorinated sepiolite (SEP-F10) enhanced the proton conductivity of the composite membrane to a level close to that of virgin Aquivion, or even slightly higher, depending on the conditions. This may account for the better compatibility between the fluorinated ionomer backbone (C-F) of Aquivion and the fluorinated groups anchored on sepiolite, thus improving the interface between the two.

The post-treatment of fluorinated sepiolite led to significantly higher proton conductivities. Both fluorinated and post-treated sepiolite (pSEP-F) were very favorable for proton conductivity: membranes prepared using 10 wt% post-treated and fluorinated sepiolite reached a proton conduction of 0.195 S/cm at 90 °C and 90% RH, while that of Aquivion was only 0.115 S/cm.

Gore Select® exhibited the best proton conductivity among selected reference membranes, two to three times that of Nafion® HP, reaching

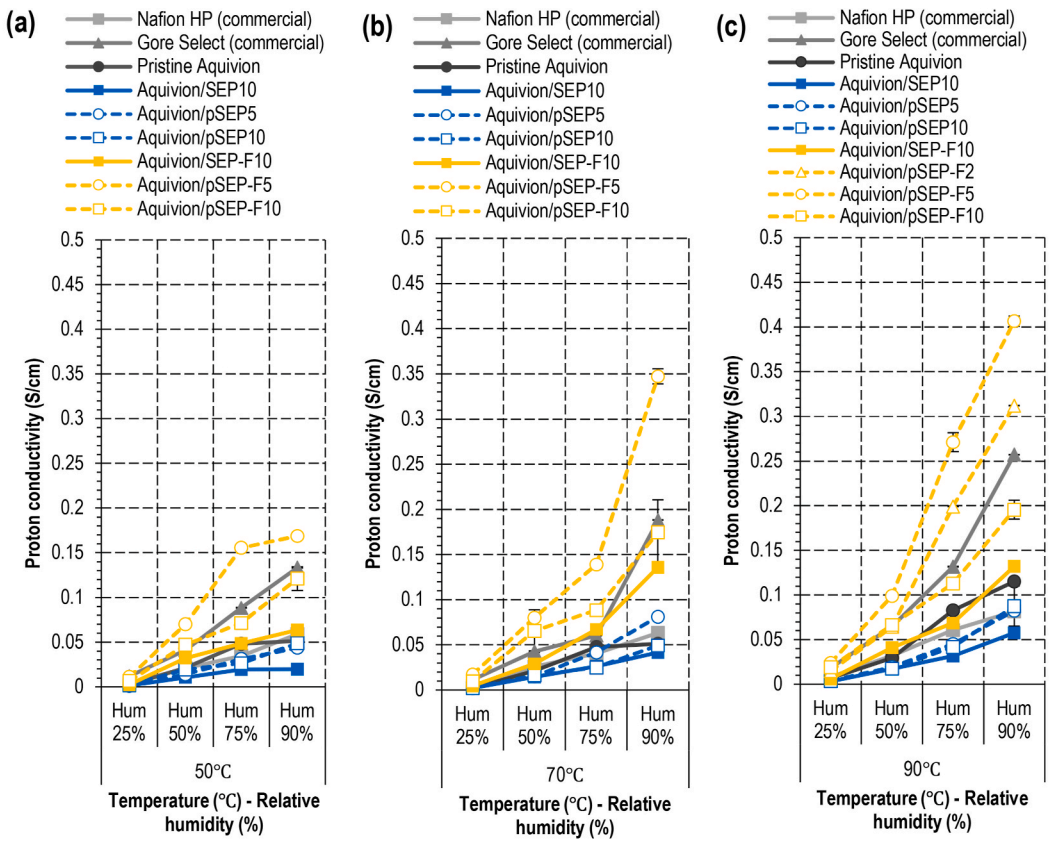

1) Gebert et al., 0.010 S/cm at 95 °C, 25% RH (Aquivion E79-03S) [67]. 2) Giancola et al., 0.118 S/cm at 80 °C, 95% RH (Aquivion EW 830 g/eq) [69]. 3) Skulimowska et al., 0.138 S/cm at 90 °C, 95% RH (Aquivion E87-12S) [68]

Fig. 6. Impact of temperature based on (a) 50 °*C*, (b) 70 °*C*, (c) 90 °*C* in various RH conditions (25, 50, 75, 90%) on proton conductivity for PEMs: Nafion HP, Gore Select (Aquivion), virgin Aquivion, Aquivion/SEP10, Aquivion/pSEP5, Aquivion/pSEP10, Aquivion/SEP-F10, Aquivion/pSEP-F2, Aquivion/pSEP-F5, and Aquivion/pSEP-F10 membranes (sepiolite = blue, fluorinated sepiolite = yellow, post-treatment = white plot and dashed line, 10 wt% = square plot, 5 wt% = circle plot, 2 wt % = triangle plot).

almost 0.260 S/cm at 90 °C and 90% RH. This stands above all the composite membranes prepared with 10 wt% sepiolites, regardless of its modification. Decreasing the amount of sepiolite to 5 wt% allowed an even higher proton conductivity of 0.407 S/cm at 90 °C and 90% RH. Further decreasing the amount of sepiolite to 2 wt% resulted in a proton conductivity of 0.310 S/cm at 90 °C and 90% RH, still higher than that of the Gore Select membrane but lower than that obtained with 5 wt% of sepiolite. It seems that there is an optimum proton conductivity at 5 wt% of incorporated sepiolite for the IEC and water uptake. This is not unexpected, as proton conductivity is highly correlated with IEC, the amount of water molecules in the membrane (RH and water uptake), and the transport of protons. The water uptake and IEC calculation for the membrane with 5% post-treatment sepiolite (pSEP5 or pSEP-F5) was slightly greater than for the membrane with 10%. Since proton conductivity is only improved with fluorinated and post-treated sepiolite (pSEP-F5), the main influence is probably the homogeneity of the dispersion, which affects the movement of protons, as discussed earlier.

Fig. S3 shows the activation energies obtained from the logarithm of proton conductivity (Arrhenius plots) as a function of various relative humidity [70].

The activation energy of the pristine Aquivion membrane was obtained to be 10.823–19.920 kJ/mol, while the commercially available membranes, Nafion HP and Gore Select, showed 11.538–18.794 kJ/mol and 8.662–16.090 kJ/mol, respectively. Membranes incorporating pristine sepiolite exhibited 13.339–21.427 kJ/mol, while incorporation of fluorinated sepiolite led to 10.307–19.544 kJ/mol. The addition of pSEP5 and pSEP10, pretreated sepiolites, displayed 11.600–21.522 kJ/mol and 11.901–20.873 kJ/mol, respectively. On the other hand, the blending of fluorinated and post-treated sepiolite reduced the activation energies (i.e., 7.437–15.534 kJ/mol for pSEP-F5 and 9.074–16.863 kJ/mol for pSEP-F10) of the membranes similarly compared to that of fluorinated sepiolite, with the lowest value among the activation energies of the tested membranes being 7.437 kJ/mol at 90 °C and 90 % RH. Based on the literature [71], the activation energy is less than 38.5 kJ/mol, suggesting that the Grotthus mechanism is the main pathway of proton transport within the ion channel of the membranes.

5.9. *Impact of fluorination and post-treatment on sepiolite*

Post-treated and fluorinated sepiolite was shown to dramatically enhance the properties of composite membranes based on Aquivion. The effects of fluorination can be attributed to better affinity of the filler with the polymer phase due to the fluorine available for interaction (Fig. 5).

Moreover, addition of fluorinated and post-treated sepiolite (pSEP-F) improves the dispersion of the nanoclays in the polymeric matrix compared to that of the non-treated sepiolite. Thus, this increases the availability of amorphous domains where the ionic conductivity mainly takes place [72,73], thereby improving the flexibility, which is in good agreement with the decreased stiffness of the membranes containing 5 wt% fluorinated and post-treated sepiolite (Fig. 5g). Ultimately, the improved side-chain flexibility of the polymer phase within the composite membranes might enhance proton transport (Fig. 8). Indeed,

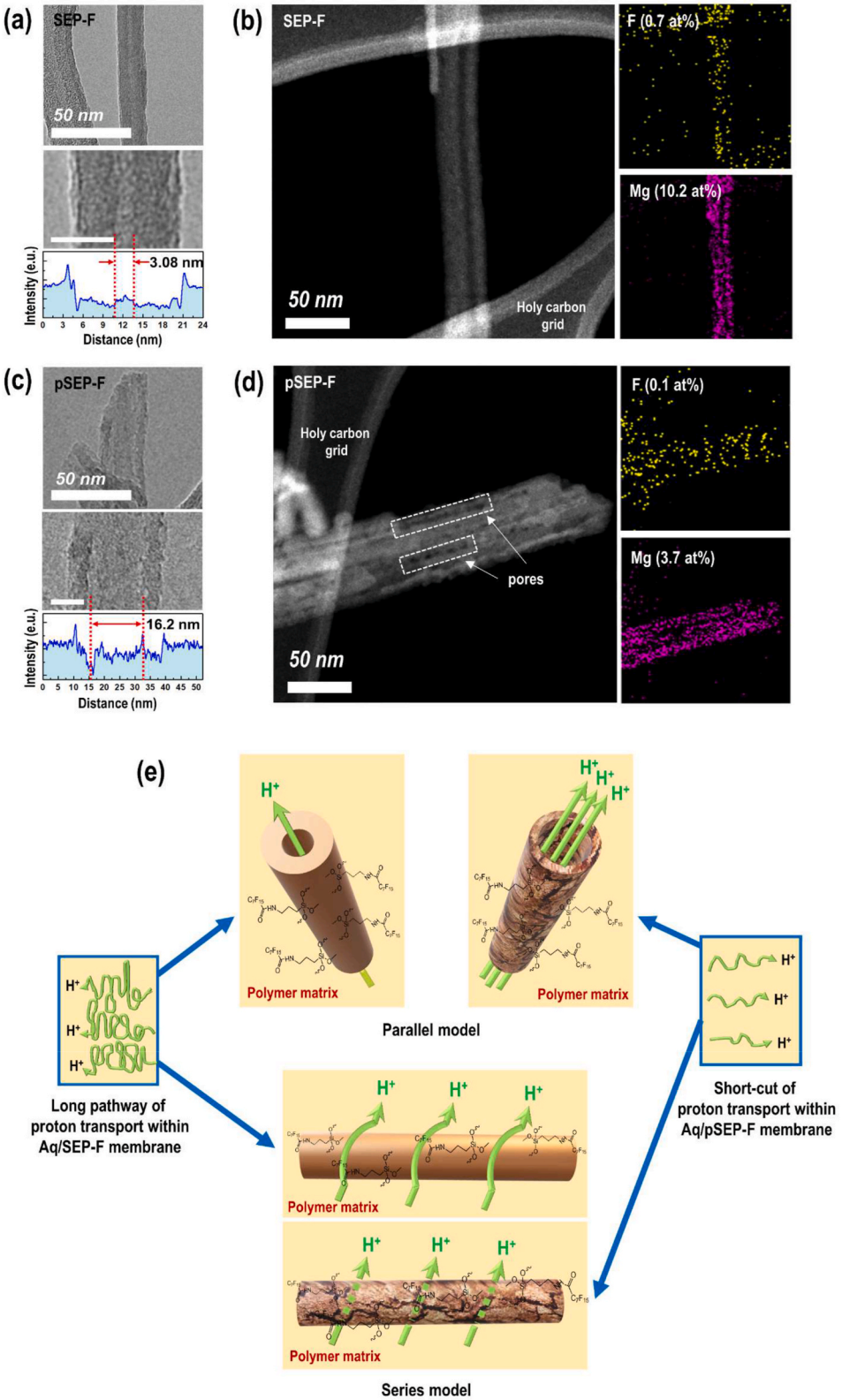

Fig. 7. TEM micrographs: line profile for lumen size measurement of (a) SEP-F and (c) pSEP-F nanofibers. STEM-EDS elemental mapping: elemental distribution and mapping for (b) SEP-F and (d) pSEP-F nanofibers. (e) conceptual proton transfer pathway through parallel or series models in composite membranes containing fluorinated and post-treated sepiolite.

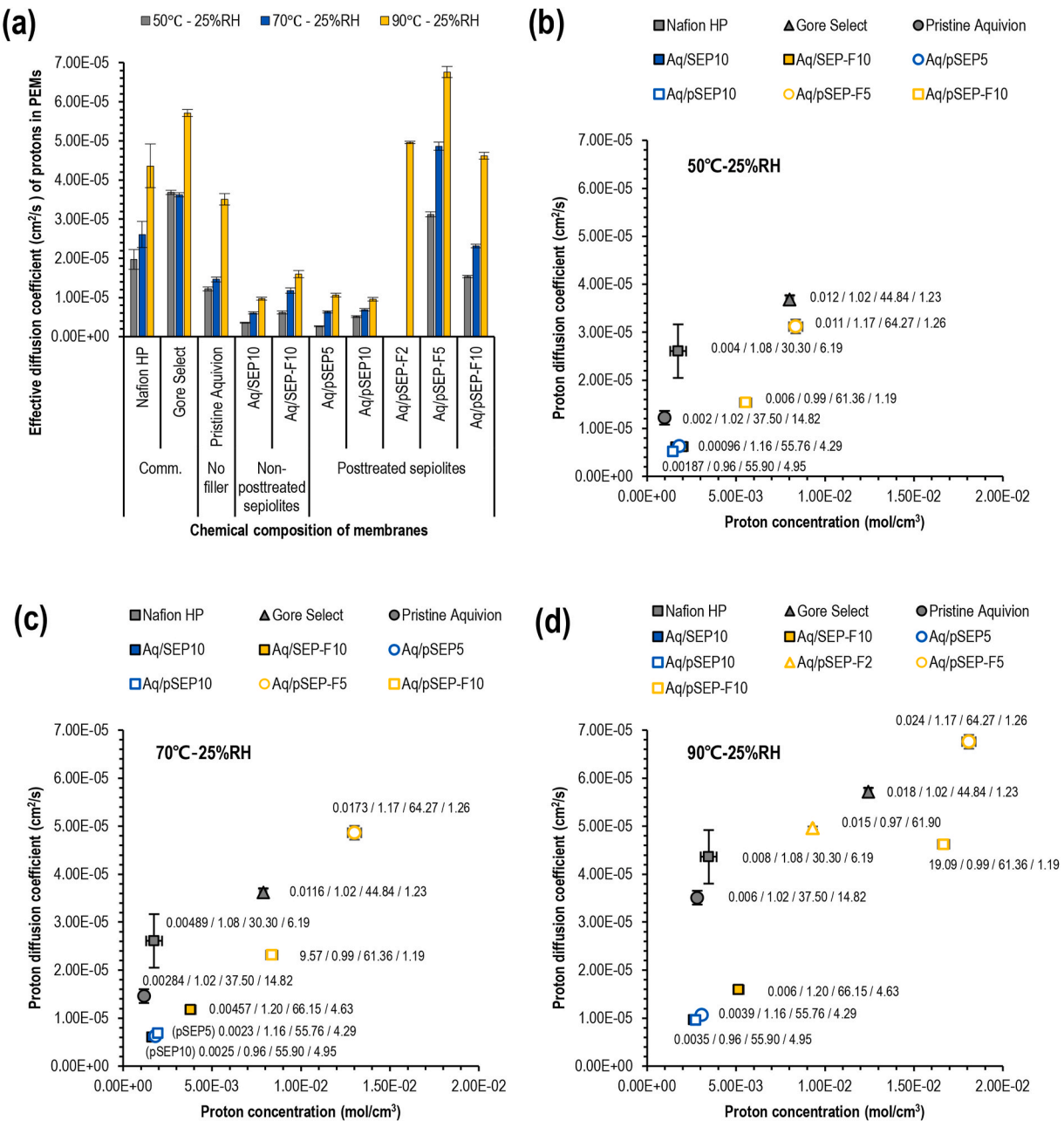

Fig. 8. Impact of fluorinated and post-treated sepiolites (pSEP-F) on composite membranes: (a, e) ionic diffusion coefficient calculated by Nernst-Einstein equation of protons in electrolyte membranes operated at 50 °*C*, 70 °*C*, and 90 °*C* under 25, 90% RH conditions, and (b to d, f to h) comparison of proton mobility from diffusion coefficient in the membranes operated at 50, 70, 90 °*C* and 25, 90% RH as a function of H^+ concentration. Yellow and blue scatter plots represent fluorinated and non-fluorinated sepiolites, respectively and white scatter plots represent post-treated sepiolites. The values next to the scatter plots represent proton conductivity (S/cm)/IEC (meq/g)/water uptake (%)/thickness swelling at boiling temperature (%).

studies have reported that the flexibility of polymer side chains affects the energy barriers for proton conductivity [74].

Another reason for the improved proton conductivity of the composite membranes with fluorinated and post-treated sepiolite is that the defects, larger pore volumes, and improved porosity (Fig. 2 and Table 2) in the sepiolite structure by the partial removal of Al_2O_3, Fe_2O_3, and MgO through post-treatment (Fig. 2fg and Fig. 3b) improved the homogeneity (Fig. 4) and water uptake (Fig. 5d). Consequently, the proton diffusion rate (i.e., diffusion coefficient) and permeation of water molecules in the amorphous structure improved. Moreover, the smaller thickness swelling (Fig. 5f) owing to the post-treatment effect minimizes the ohmic resistance. This means that improved proton conductivity was obtained depending on the change in material nanostructure, as reported in the literature [75]; thus, ion mobility is much easier. It should be noted here that the higher the ion diffusivity, the higher the ionic conductivity based on the Nernst-Einstein equation [76]. In addition, it is notable that the diffusion rate did not increase in the post-treatment of non-fluorinated sepiolite, whereas the membrane incorporated with sepiolite fluorinated and post-treated together improved the diffusion rate of protons. The reason might be that fluorine is an excellent element that enhances proton conductivity [77], as well as the interaction between fluorination and post-treatment of sepiolite.

Proton diffusion of fluorinated and post-treated sepiolite within the polymer matrix is more favorable than fluorinated sepiolite because of

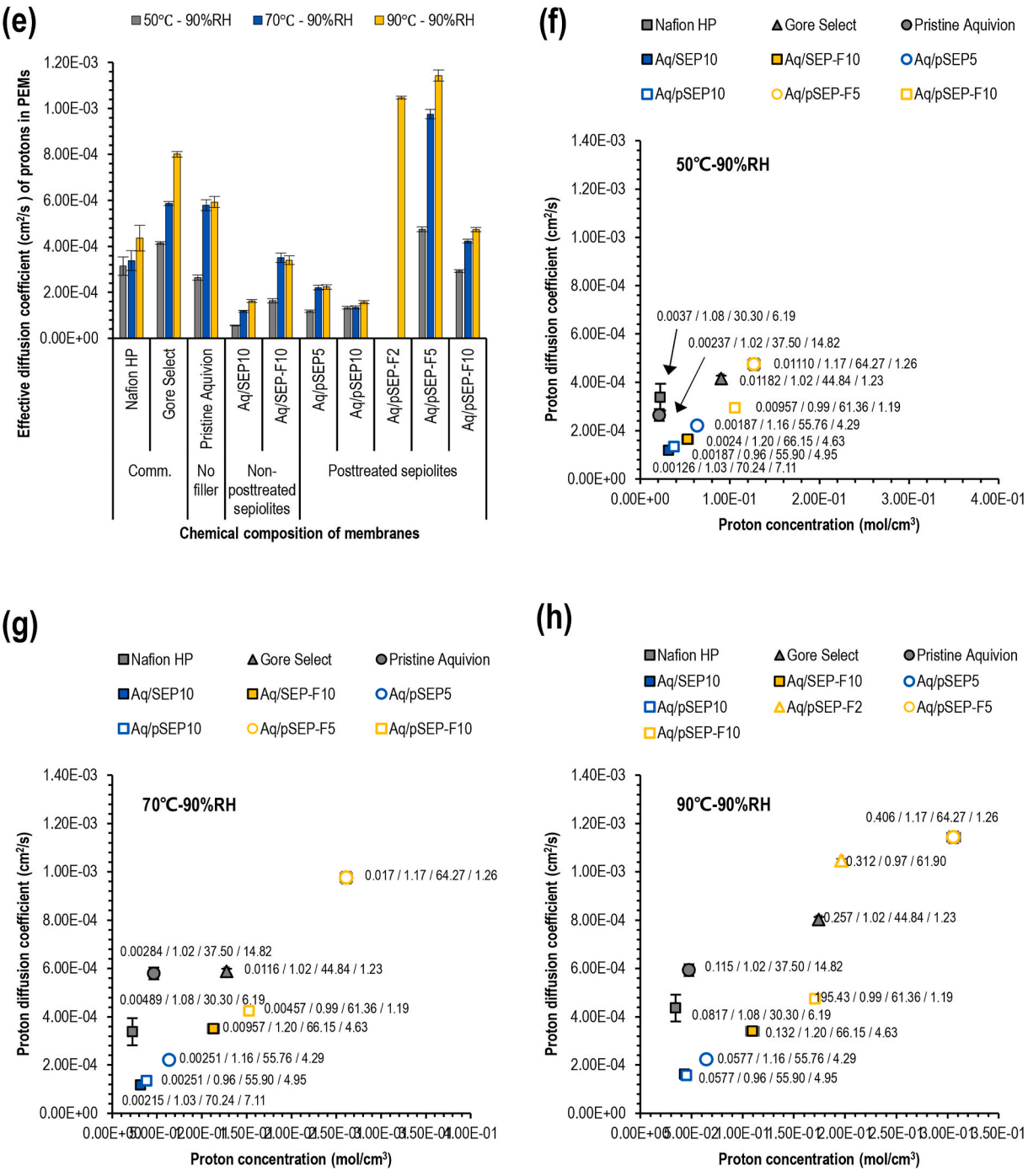

Fig. 8. (*continued*).

the wider lumen and pore volume. Increase in lumen size (i.e., 16.2 nm) and pore formation (Fig. 7d) were visually confirmed using TEM micrographs, and 0.73 $cm^3\ g^{-1}$ was also obtained by BET analysis for the total volume of fluorinated and post-treated sepiolite (Table 2). This resulted in a shorter proton transport pathway, which, in turn, facilitated better proton diffusion in the Aquivion/pSEP-F membrane. The conceptual proton transport pathway in the polymer matrix can be illustrated in Fig. 7e using the following possible mechanisms: parallel and series models [78].

Also, the rough morphology (Fig. 7d) of fluorinated and post-treated sepiolites provides the large specific surface area (193.01 $m^2\ g^{-1}$) as listed in Table 2, which increases the contact area between the polymer matrix and the sepiolite. Accordingly, sepiolite with high hygroscopicity aids in proton diffusion even under low relative humidity operating conditions. Moreover, STEM-EDS revealed that sepiolite was fluorinated both inside and outside the surface (Fig. 7b and d). Post-treatment reduced the amount of fluorine and magnesium to 0.1 at% and 3.7 at %, respectively. As a result of this impact, the surfaces of the fluorinated and post-treated sepiolites appeared rough and porous.

To confirm the proton diffusion coefficient and proton concentration of the membrane containing fluorinated and post-treated sepiolite, the Nernst-Einstein equation was used: [79].

$$D = \frac{\sigma RT}{cz^2F^2} \tag{6}$$

where σ represents the proton conductivity measured using EIS. T, R, F,

and z are the absolute temperature, ideal gas constant, Faradaic constant and valence charge, respectively. c represents the H^+ concentration calculated using Equation (7) [79].

$$c = 0.001 \times \frac{\rho \times IEC}{1 + 0.01 \times Wut_{vol}} \quad (7)$$

where ρ, IEC, and Wut_{vol} represent the polymer density, ion-exchange capacity, and volume-based water uptake, respectively.

Fig. 8a and e shows the effective diffusion coefficients of protons in the commercially available membranes and the membranes developed in this study. Generally, as the operating temperature and relative humidity increase, the effective diffusion coefficient increases.

For the 10 wt% sepiolite-loaded composite membranes, the order of the effective diffusivity of protons was as follows: Aq/SEP10 = Aq/pSEP10 < Aq/SEP-F10 < Aq < Aq/pSEP-F10. Fluorination and post-treatment of sepiolite resulted in improved proton diffusivity of the composite membrane compared to that of the Aquivion membrane.

Similar effective diffusion coefficients were obtained even when the loading of post-treated sepiolites was reduced from 10 wt% (Aq/pSEP10) to 5 wt% (Aq/pSEP5). Even after fluorination and post-treatment, loadings of 10 wt% (Aq/pSEP-F10) and 2 wt% (Aq/pSEP-F2) led to similar effective diffusion coefficients.

A higher effective diffusivity of protons was observed for Aq/pSEP-F10 and Aq/pSEP-F2 compared to pristine Aquivion. Moreover, improved effective diffusivity compared to Nafion® HP, commercially available membrane, was observed for Aq/pSEP-F composite membranes at 25, 90% RH and between 50 and 90 °C. Especially, blending with 5 wt% pSEP-F5 resulted in increased values compared to Gore Select® at 70 and 90 °C under 25, 90% RH conditions, leading to showing the best ion diffusion coefficient among the membranes tested.

Fig. 8b-d and 8f-h compare ionic mobilities of the membranes operated at 50, 70, 90 °C and 25, 90% RH as a function of proton concentration. The proton diffusion coefficient and concentration of Gore Select® improved with increasing operating temperature and relative humidity. The values of Nafion® HP were relatively lower than those of Gore Select® but were slightly higher than those of the pristine Aquivion membrane.

Incorporation of natural sepiolite or sepiolite post-treated or fluorinated alone reduced the diffusion coefficient of the composite membranes, which is lower than that of pristine Aquivion membranes, whereas similar or slightly increased proton concentrations were obtained for the membrane containing sepiolites post-treated or fluorinated alone. However, the incorporation sepiolites fluorinated and post-treated together allowed improved proton diffusivity and concentration during operation. As the operating temperature increased, better proton diffusivity and concentration were observed for the Aq/pSEP-F membranes than for the other membranes, resulting in more differences. The high proton diffusivity and concentration appear to be enhanced by the complex causes of the amorphous membrane structure, improved water uptake, and low thickness swelling at boiling temperature. At 90 °C and 90% RH, the best ionic diffusivity (1.14×10^{-3} cm^2/s) and proton concentration (3.059×10^{-1} mol/cm^3) in this work were observed, particularly when 5 wt% pSEP-F was added to Aquivion polymer matrix. In addition, this membrane showed better proton diffusivity (6.76×10^{-5} cm^2/s) and proton concentration (1.809×10^{-2} mol/cm^3) compared to others tested at 90 °C and 25% RH, suggesting that it can be used in fuel cells less sensitive to low relative humidity. Accordingly, enhanced cell performance compared to commercially available Nafion® HP and other tested membranes could be obtained for the membrane containing fluorinated and post-treated sepiolite (Aq/pSEP-F5). The fuel cell performances of PEMFCs operated under wet and dry conditions were described below.

5.10. Fuel cell performance

Under wet conditions (Fig. 9a), the voltage – current curves of Nafion® HP, pristine Aquivion, Aq/SEP10, and Aq/SEP-F10 membranes were similar. Similar mass transport losses occurred at high current densities for all the membranes, except for Nafion® HP and composite membrane containing 5% post-treated and fluorinated sepiolite. The maximum power density of pristine Aquivion was obtained at approximately 572 mW/cm^2, indicating that it is approximately 130 mW/cm^2 lower than the results reported in the literature [80]. This might be attributed to the fact that the pressure applied to our single cell in this study was set to an extreme condition of 2.5 bar (1.5 bar relative). Blending with pSEP-F5 led to a cell voltage and power density similar to that of Nafion® HP. The reason that Aq/pSEP-F5 membrane has better performance compared with pristine Aquivion and non-post-treated sepiolite-blended membranes may be attributed to: 1) reduced thickness (19.2 ± 0.1 μ m in wet state), 2) flexible side-chain polymer, and 3) promoted proton diffusivity and concentration through interaction between fluorination and post-treatment of sepiolite, thereby improving proton conductivity.

Under dry conditions (Fig. 9b), composite membranes containing non-posttreated sepiolite showed similar performance to pristine Aquivion, whereas better performance was obtained for pretreated sepiolites with fluorine groups, except for the 10 wt% loading content. Adding 5% post-treated and fluorinated sepiolite (Aq/pSEP-F5) improved performance after 0.3 A/cm^2 and better cell voltage and power density as compared to commercially available Nafion® HP and other membranes-contained MEAs.

The MEAs based on Nafion® HP and Aq/pSEP-F5 had similar performances in terms of both cell voltage and power density under wet conditions, but differed significantly in the dry state. As the current density increased under low relative humidity conditions below 30%, the performance gap between the two MEAs became more apparent. This may be due to the effect of fluorination and post-treatment on the 5 wt% sepiolite nanofiber (Aq/pSEP-F5). In other words, protons are more likely to diffuse to the Aq/pSEP-F5 membrane based on an increase in the diffusion coefficient and proton concentration, thereby showing improved performance between dry and wet conditions compared with other membranes tested. This means that pSEP-F5 contained composite membrane is less sensitive to low relative humidity and can be ultimately applied in various operating conditions with better performance. The results gathered in Fig. 9c and d indicate that the addition of 5 wt% post-treated and fluorinated sepiolites (Aq/pSEP-F5) shows the cell voltage with small gap due to the reduced MEA resistance (see Fig. S4) and good proton transport between wet and dry conditions at 0.6 A/cm^2, whereas the other membranes significantly differ in cell performance at two kinds of different operating conditions. Regarding maximum power density (Fig. 9e), the highest value was obtained for Aq/pSEP-F5-contained MEA under low relative humidity below 30% among the MEAs tested. On the other hand, the other MEAs seem to be sensitive to low relative humidity, leading to a significant difference between the dry- and wet-state operating conditions. Moreover, the output voltages for power density at 0.48 V and 0.43 V were found to be the optimal operating condition for Nafion HP and Aq/pSEP-F5, respectively (Fig. 9b).

Fig. 9f shows the maximum power densities of various MEAs compared under comparable conditions (i.e., 20–30% RH and 70–80 °C). The MEA developed by our group displayed at least 17.2–68.4% greater than the MEA with commercially available membranes (i.e., Gore Select®, Nafion® HP, Nafion® 211, Nafion® 212) for maximum power density, which has been reported in the literature [81–85]. Among the MEAs tested, Aq/pSEP-F 5 exhibited the highest power density of 700 mW/cm2. Lower values were obtained for the commercially available Gore Select® and Nafion® membrane-containing MEAs. Gore Select® and Nafion® HP showed values of approximately 580 mW/cm^2 [81], while Nafion® 211 and Nafion® 212 displayed values

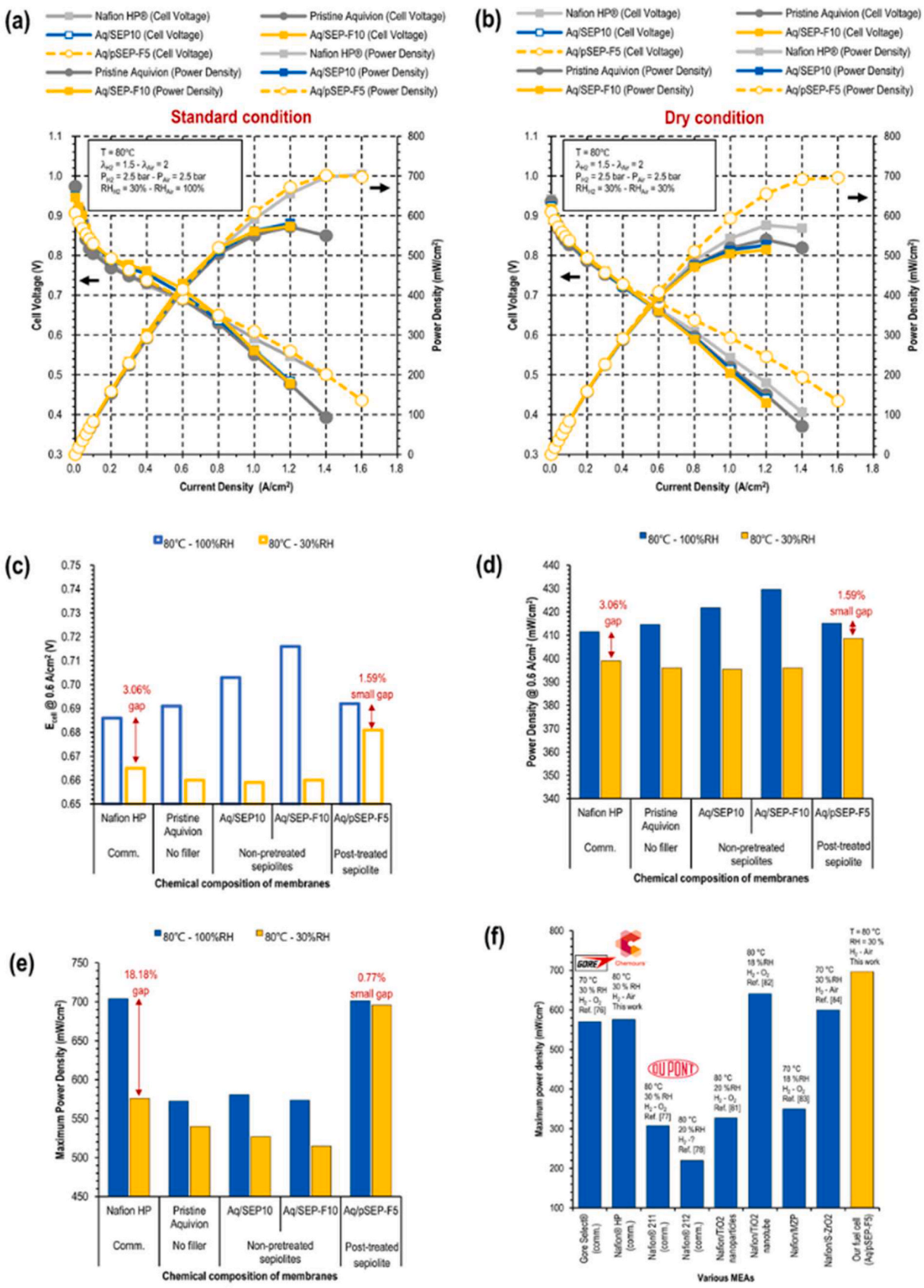

Fig. 9. Voltage – current curves and power densities of MEAs based on Nafion® HP, pristine Aquivion and Aquivion composite membranes with pure and modified sepiolites: (a) wet (RH_{H2} = 30% - RH_{Air} = 100%) and (b) dry (RH_{H2} = 30% - RH_{Air} = 30%) conditions (sepiolite = blue, fluorinated sepiolite = yellow, post-treatment = white plot and dashed line, 10 wt% = square plot, 5 wt% = circle plot). Evolution of (c) cell voltage and (d) power density at 0.6 A/cm^2, and (e) maximum power density under wet (RH_{H2} = 30% - RH_{Air} = 100%) and dry (RH_{H2} = 30% - RH_{Air} = 30%) conditions. Comparison of (f) maximum power densities (mW/cm^2) of fuel cell MEAs as reference under 18–30% RH operating conditions. Detailed information of membranes and MEA is provided in Table 3.

slightly over 200 and 300 mW/cm^2 [82,83]. Moreover, a greater maximum power density was observed for Aq/pSEP-F5 compared to Nafion composite membranes blended with TiO_2 [86,87] or ZrO_2 [88, 89]. The membrane and electrode materials, proton conductivity, and maximum power density are listed in Table 3. Membranes developed by other research groups [90–93] have not yet been reported for the maximum power density under comparable conditions; thus, cell performance cannot be compared with our MEA. It is noted here that the relationship between proton conductivity of the membranes and maximum power density of the cell is not proportional.

Hydrogen crossover is also important because it affects fuel cell efficiency. Regarding hydrogen crossover (see Fig. S5) measured under harsh operating conditions (T = 90 °C, RH = 30%, P = 3 bar), the pristine Aquivion membrane was followed by the Nafion® HP. The composite membrane had a higher hydrogen permeability compared to the pristine Aquivion and commercially available membrane. This might be attributed to the fact that the incorporated sepiolite nanofibers have relatively high hygroscopicity, so the interior of the membrane is relatively humid, allowing water to swell the membrane and widen the ion exchange channels. This is consistent with what is described in the literatures [94,95]. This was contrary to our expectation that composite membranes with improved mechanical resistance would show lower hydrogen crossover.

6. Conclusion

We developed a less sensitive proton-exchange membrane (i.e., Aq/pSEP-F5) to a relative humidity below 30%; this membrane showed a difference of only 0.77% between 100% RH and 30% RH for maximum power density.

In the study, sepiolite nanofibers were successfully functionalized with fluorine groups and post-treated with acidic solutions. Aquivion-based composite membranes were prepared by incorporating pure sepiolite (SEP) or fluorinated and post-treated sepiolite (SEP-F or pSEP-F), and their properties were compared with those of commercial membranes (i.e., Nafion® HP and Gore Select®). Several conclusions related to the physical and chemical properties of the composite membranes developed in this study can be drawn.

Adding pure sepiolite to the Aquivion matrix resulted in improved swelling ratio, water uptake, and mechanical property. The composite membrane exhibited similar chemical stability and IEC but showed reduced dispersion of fillers and proton conductivity, with greater thickness compared to Aquivion and Nafion® HP.

Incorporating fluorinated sepiolite (SEP-F) has proven to be profitable. This allowed better homogeneity inside the polymer matrix of the composite membrane. In terms of mechanical properties and ion conductivity, the prepared membranes were improved without influencing the water uptake, thickness, IEC, or chemical stability.

Regarding post-treatment impact, the composite membrane with a blend of fluorinated and post-treated sepiolite (pSEP-F) displayed IEC and chemical stability similar to commercial membranes. Moreover, the proton conductivity of the composite membrane was the highest of the membranes tested, irrespective of filler content. However, they displayed reduced thickness swelling at boiling temperature and

Table 3
Proton conductivity and maximum power density of proton exchange membranes used in hydrogen fuel cells operating at low relative humidity of 30% or below.

Sample name	Membrane material	Material for catalyst and ionomer	Proton conductivity of membrane (S/cm)	Fuel cell test			Ref.
				Feeding gas	Operating condition (RH – Temp.)	Max. power density (mW/cm^2)	
Gore Select® (Gore)	Nafion + PTFE support layer	Pt/C + ?	0.018 (25 % - 95 °C)	H_2 - O_2	30 % - 70 °C	570	[81] and this work
Nafion® HP (Chemours)	Nafion + PTFE support layer	Pt/C + Nafion® (Ion Power)	0.008 (25 % - 90 °C)	H_2 -Air	30 % - 80 °C	576	This work
Nafion® 211 (DuPont)	Nafion	Pt/C + Nafion® (Alfa Aesar)	0.012 (30 % - 80 °C)	H_2 - O_2	30 % - 80 °C	308	[82]
Nafion® 212 (DuPont)	Nafion	?	–	H_2 - ?	20 % - 80 °C	220	[83]
Aquivion® E79-03S (Solvay)	Aquivion	–	0.010 (25 % - 90 °C)	–	–	–	[67]
Aq	Aquivion	Pt/C + Nafion® (Ion Power)	0.007 (25 % - 90 °C)	H_2 -Air	30 % - 80 °C	520	This work
Aq/pSEP-F5	**Aquivion, pSEP-F5, IPA** [a]	**Pt/C + Nafion® (Ion Power)**	**0.024 (25 % - 90 °C)**	**H_2 -Air**	**30 % - 80 °C**	**696**	**This work**
Aq/HNT-SF5	Aquivion, pHNT-SF5 [b]	–	0.025 (25 % - 90 °C)	–	–	–	[40]
Nafion/TiO_2 nanoparticles	Nafion, TiO_2 nanoparticles	?	–	H_2 - O_2	20 % - 80 °C	327	[86]
Nafion/TiO_2 nanotube	Nafion, TiO_2 nanotube	Pt/C + Nafion® (Ion Power)	0.008 (18 % - 80 °C)	H_2 - O_2	18 % - 80 °C	641	[87]
Nafion/MZP	Nafion, MZP [c]	Pt/C + Nafion® (DuPont)	0.017 (30 % - 70 °C)	H_2 - O_2	18 % - 70 °C	350	[88]
Nafion/S-ZrO_2	Nafion, S-ZrO_2	Pt/C + ?	–	H_2 -Air	30 % - 70 °C	600	[89]
N/SWy−oxCNT−RSO_3H(y5) Nafion	Nafion, Montmorillonite/CNT [d]	–	0.035 (30 % - 90 °C)	–	–	–	[90]
NIM-SO_3 Nafion	Nafion, NIM_SO_3 [e]	–	0.031 (30 % - 90 °C)	–	–	–	[91]
Composite	Nafion, MCM-41 [f], DMF [g]	–	0.071 (20 % - 80 °C)	–	–	–	[92]
Silane based nanostructured composite membrane	GPTMS [h], EHTES [i], H_3PO_4, Cloisite® 30B	–	0.023 (30 % - 80 °C)	–	–	–	[93]

[a] Isopropyl alcohol.
[b] Halloysite nanotube modified with Sodium 2,3-dihydroxynaphthalene-6-sulfonate and N-(3-triethoxysilylpropyl)perfluorooctanoamide.
[c] Mesoporous zirconium phosphate.
[d] Carbon nanotube.
[e] Sulfonate modified silica nanoparticles.
[f] Silica filler modified with sodium hydroxide, cetyltrimethylammonium bromide, and tetraethoxysilane.
[g] Dimethylformamide.
[h] 3-glycidoxy propyl trimethoxy silane.
[i] 2 (3, 4 epoxy cyclohexyl) ethyl triethoxy silane.

mechanical strength. Enhanced proton diffusion coefficients and proton concentrations were also observed by adding 5 or 10 wt% fluorinated and post-treated sepiolite, which resulted from the amorphous structure, improved water uptake, and low swelling at the boiling temperature of the composite membrane. Cell performance was also observed for MEAs containing the membranes developed in this study. A slightly enhanced performance at 0.6 A/cm^2 was obtained for fluorinated sepiolite-based membranes compared to pristine Aquivion or Nafion® HP, particularly at intermediate current densities, under wet conditions. The best cell voltage and power density were achieved with the composite membrane containing fluorinated and post-treated sepiolite (i.e., Aq/pSEP-F5) among the membranes tested under dry conditions. Even, Aq/pSEP-F5 membrane was found to be less sensitive to low relative humidity below 30% because of small difference between wet and dry operating conditions.

Based on characterization, blending with 5% fluorinated and post-treated sepiolite may be a viable route for improving the physico-chemical properties of fabricated membranes, leading to a good result on hydrogen fuel cell performance at low relative humidity.

CRediT authorship contribution statement

Sahng Hyuck Woo: Writing – review & editing. **Belkacem Otazaghine:** Writing – original draft, Data curation, Conceptualization. **Sara Cavaliere:** Data curation, Conceptualization. **Byeong-Seon An:** Formal analysis. **Hee Soo Kim:** Formal analysis, Conceptualization. **Jae-Hun Kim:** Data curation, Conceptualization. **Young-Gi Yoon:** Data curation, Conceptualization. **Soo Youn Lee:** Conceptualization. **Arnaud Rigacci:** Data curation, Conceptualization. **Christian Beauger:** Writing – review & editing, Writing – original draft, Investigation, Funding acquisition, Formal analysis, Data curation, Conceptualization.

Declaration of competing interest

The authors declare that they have no known competing financial interests or personal relationships that could have appeared to influence the work reported in this paper.

Data availability

Data will be made available on request.

Acknowledgements

The authors wish to thank Pierre Ilbizian (PERSEE center), Patrick Leroux (PERSEE center), Cedric Sernissi (PERSEE center), Gabriel Monge (CEMEF center), Suzanne Jacomet (CEMEF center), Aurélie Taguet (C2MA center), Benjamin Gallard (C2MA center), and Loc Dumazert (C2MA center) for technical support. This study was supported by funding from the COMEHTE project (contract number ANR-15-CE05-0025-01) granted by the French National Research Agency (ANR). This work was partially supported by the Research and Development Program of the Korea Institute of Energy Research (KIER) (C2-2422-01, C2-2471). This research also supported by Korea Ministry of Environment (MOE; 2021003240005) which are greatly appreciated. This research was conducted under the Bio & Medical Technology Development Program of the National Research Foundation (NRF) through the project of Consolidated e-Biorefinery of lignocellulosic biomass funded by the Korean government (MSIT; 2022M3A9F3082335).

Appendix A. Supplementary data

Supplementary data to this article can be found online at https://doi.org/10.1016/j.memsci.2024.122574.

References

[1] M. Winter, R.J. Brodd, What Are Batteries, Fuel Cells, and Supercapacitors? ACS Publications, 2004.
[2] B.C. Steele, A. Heinzel, Materials for fuel-cell technologies, materials for sustainable energy: a collection of peer-reviewed research and review articles from nature publishing group, World Scientific (2011) 224–231.
[3] J.-M. Thomassin, C. Pagnoulle, D. Bizzari, G. Caldarella, A. Germain, R. Jérôme, Improvement of the barrier properties of Nafion® by fluoro-modified montmorillonite, Solid State Ionics 177 (13–14) (2006) 1137–1144.
[4] K. Kreuer, On the development of proton conducting polymer membranes for hydrogen and methanol fuel cells, J. Membr. Sci. 185 (1) (2001) 29–39.
[5] J. Li, M. Pan, H. Tang, Understanding short-side-chain perfluorinated sulfonic acid and its application for high temperature polymer electrolyte membrane fuel cells, RSC Adv. 4 (8) (2014) 3944–3965.
[6] A. Stassi, I. Gatto, E. Passalacqua, V. Antonucci, A. Arico, L. Merlo, C. Oldani, E. Pagano, Performance comparison of long and short-side chain perfluorosulfonic membranes for high temperature polymer electrolyte membrane fuel cell operation, J. Power Sources 196 (21) (2011) 8925–8930.
[7] A. Aricò, A. Di Blasi, G. Brunaccini, F. Sergi, G. Dispenza, L. Andaloro, M. Ferraro, V. Antonucci, P. Asher, S. Buche, High temperature operation of a solid polymer electrolyte fuel cell stack based on a new ionomer membrane, Fuel Cell. 10 (6) (2010) 1013–1023.
[8] A.-C. Dupuis, Proton exchange membranes for fuel cells operated at medium temperatures: materials and experimental techniques, Prog. Mater. Sci. 56 (3) (2011) 289–327.
[9] A. Chandan, M. Hattenberger, A. El-Kharouf, S. Du, A. Dhir, V. Self, B.G. Pollet, A. Ingram, W. Bujalski, High temperature (HT) polymer electrolyte membrane fuel cells (PEMFC)–A review, J. Power Sources 231 (2013) 264–278.
[10] S. Peighambardoust, S. Rowshanzamir, M. Amjadi, Review of the proton exchange membranes for fuel cell applications, Int. J. Hydrogen Energy 35 (17) (2010) 9349–9384.
[11] D.J. Kim, M.J. Jo, S.Y. Nam, A review of polymer–nanocomposite electrolyte membranes for fuel cell application, J. Ind. Eng. Chem. 21 (2015) 36–52.
[12] P. Kongkachuichay, S. Pimprom, Nafion/Analcime and Nafion/Faujasite composite membranes for polymer electrolyte membrane fuel cells, Chem. Eng. Res. Des. 88 (4) (2010) 496–500.
[13] E. Şengül, H. Erdener, R.G. Akay, H. Yücel, N. Bac, İ. Eroğlu, Effects of sulfonated polyether-etherketone (SPEEK) and composite membranes on the proton exchange membrane fuel cell (PEMFC) performance, Int. J. Hydrogen Energy 34 (10) (2009) 4645–4652.
[14] B.P. Tripathi, M. Kumar, V.K. Shahi, Highly stable proton conducting nanocomposite polymer electrolyte membrane (PEM) prepared by pore modifications: an extremely low methanol permeable PEM, J. Membr. Sci. 327 (1–2) (2009) 145–154.
[15] A. Carbone, A. Saccà, I. Gatto, R. Pedicini, E. Passalacqua, Investigation on composite S-PEEK/H-BETA MEAs for medium temperature PEFC, Int. J. Hydrogen Energy 33 (12) (2008) 3153–3158.
[16] R. Nagarale, W. Shin, P.K. Singh, Progress in ionic organic-inorganic composite membranes for fuel cell applications, Polym. Chem. 1 (4) (2010) 388–408.
[17] A.K. Mishra, S. Bose, T. Kuila, N.H. Kim, J.H. Lee, Silicate-based polymer-nanocomposite membranes for polymer electrolyte membrane fuel cells, Prog. Polym. Sci. 37 (6) (2012) 842–869.
[18] W. Zhengbang, H. Tang, P. Mu, Self-assembly of durable Nafion/TiO2 nanowire electrolyte membranes for elevated-temperature PEM fuel cells, J. Membr. Sci. 369 (1–2) (2011) 250–257.
[19] B. Matos, E. Aricó, M. Linardi, A. Ferlauto, E. Santiago, F. Fonseca, Thermal properties of Nafion–TiO2 composite electrolytes for PEM fuel cell, Journal of thermal analysis and calorimetry 97 (2) (2009) 591.
[20] V. Di Noto, R. Gliubizzi, E. Negro, G. Pace, Effect of SiO2 on relaxation phenomena and mechanism of ion conductivity of [Nafion/(SiO2) x] composite membranes, J. Phys. Chem. B 110 (49) (2006) 24972–24986.
[21] F. Pereira, K. Vallé, P. Belleville, A. Morin, S. Lambert, C. Sanchez, Advanced mesostructured hybrid silica− nafion membranes for high-performance PEM fuel cell, Chem. Mater. 20 (5) (2008) 1710–1718.
[22] N.H. Jalani, K. Dunn, R. Datta, Synthesis and characterization of Nafion®-MO2 (M= Zr, Si, Ti) nanocomposite membranes for higher temperature PEM fuel cells, Electrochim. Acta 51 (3) (2005) 553–560.
[23] A. Saccà, A. Carbone, R. Pedicini, M. Marrony, R. Barrera, M. Elomaa, E. Passalacqua, Phosphotungstic acid supported on a nanopowdered ZrO2 as a filler in nafion-based membranes for polymer electrolyte fuel cells, Fuel Cell. 8 (3-4) (2008) 225–235.
[24] A. D'Epifanio, M.A. Navarra, F.C. Weise, B. Mecheri, J. Farrington, S. Licoccia, S. Greenbaum, Composite nafion/sulfated zirconia membranes: effect of the filler surface properties on proton transport characteristics, Chem. Mater. 22 (3) (2009) 813–821.
[25] Y. Zhai, H. Zhang, J. Hu, B. Yi, Preparation and characterization of sulfated zirconia (SO42−/ZrO2)/Nafion composite membranes for PEMFC operation at high temperature/low humidity, J. Membr. Sci. 280 (1–2) (2006) 148–155.
[26] A. Filippov, D. Khanukaeva, D. Afonin, G. Skorikova, E. Ivanov, V. Vinokurov, Y. Lvov, Transport properties of novel hybrid cation-exchange membranes on the base of MF-4SC and halloysite nanotubes, J. Mater. Sci. Chem. Eng. 3 (1) (2015) 58.
[27] G. Cavallaro, R. De Lisi, G. Lazzara, S. Milioto, Polyethylene glycol/clay nanotubes composites, Journal of thermal analysis and calorimetry 112 (1) (2013) 383–389.

[28] M. Oroujzadeh, S. Mehdipour-Ataei, M. Esfandeh, Microphase separated sepiolite-based nanocomposite blends of fully sulfonated poly (ether ketone)/non-sulfonated poly (ether sulfone) as proton exchange membranes from dual electrospun mats, RSC Adv. 5 (88) (2015) 72075–72083.
[29] F.J. Fernandez-Carretero, K. Suarez, O. Solorza, E. Riande, V. Compan, PEMFC performance of MEAs based on Nafion® and sPSEBS hybrid membranes, J. N. Mater. Electrochem. Syst. 13 (3) (2010) 191–199.
[30] P. Bébin, M. Caravanier, H. Galiano, Nafion®/clay-SO3H membrane for proton exchange membrane fuel cell application, J. Membr. Sci. 278 (1–2) (2006) 35–42.
[31] J.-H. Chang, J.H. Park, G.-G. Park, C.-S. Kim, O.O. Park, Proton-conducting composite membranes derived from sulfonated hydrocarbon and inorganic materials, J. Power Sources 124 (1) (2003) 18–25.
[32] I. Nicotera, A. Enotiadis, K. Angjeli, L. Coppola, D. Gournis, Evaluation of smectite clays as nanofillers for the synthesis of nanocomposite polymer electrolytes for fuel cell applications, Int. J. Hydrogen Energy 37 (7) (2012) 6236–6245.
[33] F. Mura, R. Silva, A. Pozio, Study on the conductivity of recast Nafion®/montmorillonite and Nafion®/TiO2 composite membranes, Electrochim. Acta 52 (19) (2007) 5824–5828.
[34] K. Fatyeyeva, J. Bigarré, B. Blondel, H. Galiano, D. Gaud, M. Lecardeur, F. Poncin-Epaillard, Grafting of p-styrene sulfonate and 1, 3-propane sultone onto Laponite for proton exchange membrane fuel cell application, J. Membr. Sci. 366 (1–2) (2011) 33–42.
[35] C. Beauger, G. Lainé, A. Burr, A. Taguet, B. Otazaghine, Improvement of Nafion®-sepiolite composite membranes for PEMFC with sulfo-fluorinated sepiolite, J. Membr. Sci. 495 (2015) 392–403.
[36] C. Beauger, G. Lainé, A. Burr, A. Taguet, B. Otazaghine, A. Rigacci, Nafion®–sepiolite composite membranes for improved proton exchange membrane fuel cell performance, J. Membr. Sci. 430 (2013) 167–179.
[37] H. Zhang, T. Zhang, J. Wang, F. Pei, Y. He, J. Liu, Enhanced proton conductivity of sulfonated poly (ether ether ketone) membrane embedded by dopamine-modified nanotubes for proton exchange membrane fuel cell, Fuel Cell. 13 (6) (2013) 1155–1165.
[38] A.K. Mishra, T. Kuila, N.H. Kim, J.H. Lee, Effect of peptizer on the properties of Nafion–Laponite clay nanocomposite membranes for polymer electrolyte membrane fuel cells, J. Membr. Sci. 389 (2012) 316–323.
[39] S.H. Woo, A. Taguet, B. Otazaghine, A. Mosdale, A. Rigacci, C. Beauger, Physicochemical properties of Aquivion/fluorine grafted sepiolite electrolyte membranes for use in PEMFC, Electrochim. Acta 319 (2019) 933–946.
[40] S.H. Woo, A. Taguet, B. Otazaghine, A. Akrout, S. Cavaliere, A. Rigacci, C. Beauger, Composite short-side-chain PFSA electrolyte membranes containing selectively modified halloysite nanotubes (HNTs), J. Mater. Sci. 56 (23) (2021) 13108–13127.
[41] X. Liu, S. He, G. Song, H. Jia, Z. Shi, S. Liu, L. Zhang, J. Lin, S. Nazarenko, Proton conductivity improvement of sulfonated poly (ether ether ketone) nanocomposite membranes with sulfonated halloysite nanotubes prepared via dopamine-initiated atom transfer radical polymerization, J. Membr. Sci. 504 (2016) 206–219.
[42] M.-K. Song, S.-B. Park, Y.-T. Kim, K.-H. Kim, S.-K. Min, H.-W. Rhee, Characterization of polymer-layered silicate nanocomposite membranes for direct methanol fuel cells, Electrochim. Acta 50 (2–3) (2004) 639–643.
[43] J.-M. Thomassin, C. Pagnoulle, G. Caldarella, A. Germain, R. Jérôme, Contribution of nanoclays to the barrier properties of a model proton exchange membrane for fuel cell application, J. Membr. Sci. 270 (1–2) (2006) 50–56.
[44] I.-M. Low, A. Hakamy, F. Shaikh, High Performance Natural Fiber-Nanoclay Reinforced Cement Nanocomposites, Springer, 2017.
[45] A. Rico-Zavala, F.V. Matera, N. Arjona, J. Rodríguez-Morales, J. Ledesma-Garcia, M. Gurrola, L. Arriaga, Nanocomposite membrane based on SPEEK as a perspectives application in electrochemical hydrogen compressor, Int. J. Hydrogen Energy 44 (10) (2019) 4839–4850.
[46] F. Fernandez-Carretero, V. Compan, E. Riande, Hybrid ion-exchange membranes for fuel cells and separation processes, J. Power Sources 173 (1) (2007) 68–76.
[47] S.H. Woo, A. Rigacci, C. Beauger, Influence of sepiolite and halloysite nanoclay additives on the water uptake and swelling of Nafion based composite membranes for PEMFC: impact of the blending time on composite homogeneity, Chem. Lett. 48 (5) (2019) 418–421.
[48] S. Lazarević, I. Janković-Častvan, D. Jovanović, S. Milonjić, D. Janaćković, R. Petrović, Adsorption of Pb2+, Cd2+ and Sr2+ ions onto natural and acid-activated sepiolites, Appl. Clay Sci. 37 (1–2) (2007) 47–57.
[49] M.S. Barrios, L.F. González, M.V. Rodríguez, J.M. Pozas, Acid activation of a palygorskite with HCl: development of physico-chemical, textural and surface properties, Appl. Clay Sci. 10 (3) (1995) 247–258.
[50] L. Gozalez, L. Ibarra, A. Rodriguez, J. Moya, F. Valle, Fibrous silica gel obtained from sepiolite by HCl attack, Clay Miner. 19 (1) (1984) 93–98.
[51] A. Jiménez-López, J.d.D. López-González, A. Ramírez-Sāenz, F. Rodrīguez-Reinoso, C. Valenzuela-Calahorro, L. Zurita-Herrera, Evolution of surface area in a sepiolite as a function of acid and heat treatments, Clay Miner. 13 (4) (1978) 375–385.
[52] A. Esteban-Cubillo, R. Pina-Zapardiel, J. Moya, M. Barba, C. Pecharromán, The role of magnesium on the stability of crystalline sepiolite structure, J. Eur. Ceram. Soc. 28 (9) (2008) 1763–1768.
[53] J. Qiao, M. Saito, K. Hayamizu, T. Okada, Degradation of perfluorinated ionomer membranes for PEM fuel cells during processing with H2O2, J. Electrochem. Soc. 153 (6) (2006) A967–A974.
[54] Q. Guo, P.N. Pintauro, H. Tang, S. O'Connor, Sulfonated and crosslinked polyphosphazene-based proton-exchange membranes, J. Membr. Sci. 154 (2) (1999) 175–181.
[55] F.N. Büchi, B. Gupta, O. Haas, G.G. Scherer, Study of radiation-grafted FEP-G-polystyrene membranes as polymer electrolytes in fuel cells, Electrochim. Acta 40 (3) (1995) 345–353.
[56] J. Xie, D.L. Wood, D.M. Wayne, T.A. Zawodzinski, P. Atanassov, R.L. Borup, Durability of PEFCs at high humidity conditions, J. Electrochem. Soc. 152 (1) (2005) A104–A113.
[57] M.S. del Río, E. García-Romero, M. Suárez, I. da Silva, L. Fuentes-Montero, G. Martínez-Criado, Variability in sepiolite: diffraction studies, Am. Mineral. 96 (10) (2011) 1443–1454.
[58] K. Chemizmu, R. Fentona, Fenton reaction-controversy concerning the chemistry, Ecological chemistry and engineering 16 (2009) 347–358.
[59] W. Barb, J. Baxendale, P. George, K. Hargrave, Reactions of ferrous and ferric ions with hydrogen peroxide. Part I.—the ferrous ion reaction, Trans. Faraday Soc. 47 (1951) 462–500.
[60] A. Yebra-Rodriguez, J. Martin-Ramos, F. Del Rey, C. Viseras, A. Lopez-Galindo, Effect of acid treatment on the structure of sepiolite, Clay Miner. 38 (3) (2003) 353–360.
[61] A.S. Aricò, V. Baglio, V. Antonucci, Composite membranes for high temperature direct methanol fuel cells, Membranes for Energy Conversion 2 (2007) 123–167.
[62] L. Liang, Effects of Surface Chemistry on Kinetics of Coagulation of Submicron Iron Oxide Particles ([alpha]-Fe2O3) in Water, California Institute of Technology, 1988.
[63] C. Zhao, H. Lin, K. Shao, X. Li, H. Ni, Z. Wang, H. Na, Block sulfonated poly (ether ether ketone) s (SPEEK) ionomers with high ion-exchange capacities for proton exchange membranes, J. Power Sources 162 (2) (2006) 1003–1009.
[64] N. Agmon, The grotthuss mechanism, Chem. Phys. Lett. 244 (5–6) (1995) 456–462.
[65] K.D. Kreuer, A. Rabenau, W. Weppner, Vehicle mechanism, a new model for the interpretation of the conductivity of fast proton conductors, Angew. Chem. Int. Ed. 21 (3) (1982) 208–209.
[66] H. Zhang, C. Ma, J. Wang, X. Wang, H. Bai, J. Liu, Enhancement of proton conductivity of polymer electrolyte membrane enabled by sulfonated nanotubes, Int. J. Hydrogen Energy 39 (2) (2014) 974–986.
[67] M. Gebert, A. Ghielmi, L. Merlo, M. Corasaniti, V. Arcella, AQUIVION {trade mark, serif}–the short-side-chain and low-EW PFSA for next-generation PEFCs expands production and utilization, ECS Trans. 26 (1) (2010) 279–283.
[68] A. Skulimowska, M. Dupont, M. Zaton, S. Sunde, L. Merlo, D.J. Jones, J. Rozière, Proton exchange membrane water electrolysis with short-side-chain Aquivion® membrane and IrO2 anode catalyst, Int. J. Hydrogen Energy 39 (12) (2014) 6307–6316.
[69] S. Giancola, M. Zatoń, Á. Reyes-Carmona, M. Dupont, A. Donnadio, S. Cavaliere, J. Rozière, D.J. Jones, Composite short side chain PFSA membranes for PEM water electrolysis, J. Membr. Sci. 570 (2019) 69–76.
[70] Y. Jun, H. Zarrin, M. Fowler, Z. Chen, Functionalized titania nanotube composite membranes for high temperature proton exchange membrane fuel cells, Int. J. Hydrogen Energy 36 (10) (2011) 6073–6081.
[71] Y. Yagizatli, B. Ulas, A. Sahin, I. Ar, Investigation of sulfonation reaction kinetics and effect of sulfonation degree on membrane characteristics for PEMFC performance, Ionics 28 (5) (2022) 2323–2336.
[72] J. Jaafar, A. Ismail, T. Matsuura, K. Nagai, Performance of SPEEK based polymer–nanoclay inorganic membrane for DMFC, J. Membr. Sci. 382 (1–2) (2011) 202–211.
[73] K.S. Roelofs, T. Hirth, T. Schiestel, Sulfonated poly (ether ether ketone)-based silica nanocomposite membranes for direct ethanol fuel cells, J. Membr. Sci. 346 (1) (2010) 215–226.
[74] J.K. Clark, S.J. Paddison, Side chain flexibility in perfluorosulfonic acid ionomers: an ab initio study, J. Phys. Chem. 117 (40) (2013) 10534–10543.
[75] D.K. Paul, R. McCreery, K. Karan, Proton transport property in supported Nafion nanothin films by electrochemical impedance spectroscopy, J. Electrochem. Soc. 161 (14) (2014) F1395.
[76] O. Sel, L. To Thi Kim, C. Debiemme-Chouvy, C. Gabrielli, C. Laberty-Robert, H. Perrot, Determination of the diffusion coefficient of protons in Nafion thin films by ac-electrogravimetry, Langmuir 29 (45) (2013) 13655–13660.
[77] G.C. Maiti, F. Freund, Influence of fluorine substitution on the proton conductivity of hydroxyapatite, J. Chem. Soc., Dalton Trans. 4 (1981) 949–955.
[78] J.-H. Seol, J.-H. Won, M.-S. Lee, K.-S. Yoon, Y.T. Hong, S.-Y. Lee, A proton conductive silicate-nanoencapsulated polyimide nonwoven as a novel porous substrate for a reinforced sulfonated poly (arylene ether sulfone) composite membrane, J. Mater. Chem. 22 (4) (2012) 1634–1642.
[79] J. Pan, L. Zhu, J. Han, M.A. Hickner, Mechanically tough and chemically stable anion exchange membranes from rigid-flexible semi-interpenetrating networks, Chem. Mater. 27 (19) (2015) 6689–6698.
[80] S. Paul, S.-J. Choi, H.J. Kim, Enhanced proton conductivity of a Zn (II)-based MOF/aquivion composite membrane for PEMFC applications, Energy & Fuels 34 (8) (2020) 10067–10077.
[81] M. Wang, W. Ma, C. Yang, Z. Xia, S. Wang, G. Sun, Study on fiber-reinforced proton exchange membrane using high-surface-energy substrate, J. Membr. Sci. 647 (2022) 119940.
[82] J. Peron, A. Mani, X. Zhao, D. Edwards, M. Adachi, T. Soboleva, Z. Shi, Z. Xie, T. Navessin, S. Holdcroft, Properties of Nafion® NR-211 membranes for PEMFCs, J. Membr. Sci. 356 (1–2) (2010) 44–51.
[83] Y. Kim, K. Ketpang, S. Jaritphun, J.S. Park, S. Shanmugam, A polyoxometalate coupled graphene oxide–Nafion composite membrane for fuel cells operating at low relative humidity, J. Mater. Chem. A 3 (15) (2015) 8148–8155.
[84] C. Lee, H. Na, Y. Jeon, H.J. Hwang, H.-J. Kim, I. Mochida, S.-H. Yoon, J.-I. Park, Y.-G. Shul, Poly (ether imide) nanofibrous web composite membrane with SiO2/heteropolyacid ionomer for durable and high-temperature polymer electrolyte membrane (PEM) fuel cells, J. Ind. Eng. Chem. 74 (2019) 7–13.
[85] H. Ito, T. Mimoto, S. Someya, T. Munakata, Net water drag coefficient during high temperature operation of polymer electrolyte fuel cells, J. Electrochem. Soc. 168 (12) (2021) 124505.

[86] R.R. Abbaraju, N. Dasgupta, A.V. Virkar, Composite Nafion membranes containing nanosize TiO2/ SnO2 for proton exchange membrane fuel cells, J. Electrochem. Soc. 155 (12) (2008) B1307.
[87] K. Ketpang, K. Lee, S. Shanmugam, Facile synthesis of porous metal oxide nanotubes and modified Nafion composite membranes for polymer electrolyte fuel cells operated under low relative humidity, ACS applied materials & interfaces 6 (19) (2014) 16734–16744.
[88] A. Sahu, S. Pitchumani, P. Sridhar, A. Shukla, Co-assembly of a nafion–mesoporous zirconium phosphate composite membrane for PEM fuel cells, Fuel Cell. 9 (2) (2009) 139–147.
[89] A. D'Epifanio, M.A. Navarra, F.C. Weise, B. Mecheri, J. Farrington, S. Licoccia, S. Greenbaum, Composite nafion/sulfated zirconia membranes: effect of the filler surface properties on proton transport characteristics, Chem. Mater. 22 (3) (2010) 813–821.
[90] C. Simari, G. Potsi, A. Policicchio, I. Perrotta, I. Nicotera, Clay–carbon nanotubes hybrid materials for nanocomposite membranes: advantages of branched structure for proton transport under low humidity conditions in PEMFCs, J. Phys. Chem. C 120 (5) (2016) 2574–2584.
[91] L.G. Boutsika, A. Enotiadis, I. Nicotera, C. Simari, G. Charalambopoulou, E. P. Giannelis, T. Steriotis, Nafion® nanocomposite membranes with enhanced properties at high temperature and low humidity environments, Int. J. Hydrogen Energy 41 (47) (2016) 22406–22414.
[92] Y. Jin, S. Qiao, L. Zhang, Z.P. Xu, S. Smart, J.C.D. da Costa, G.Q. Lu, Novel Nafion composite membranes with mesoporous silica nanospheres as inorganic fillers, J. Power Sources 185 (2) (2008) 664–669.
[93] R. Jana, H. Bhunia, Thermal stability and proton conductivity of silane based nanostructured composite membranes, Solid State Ionics 178 (37–38) (2008) 1872–1878.
[94] S. Kim, B.T.D. Nguyen, H. Ko, M. Kim, K. Kim, S. Nam, J.F. Kim, Accurate evaluation of hydrogen crossover in water electrolysis systems for wetted membranes, Int. J. Hydrogen Energy 46 (29) (2021) 15135–15144.
[95] Q. Tang, B. Li, D. Yang, P. Ming, C. Zhang, Y. Wang, Review of hydrogen crossover through the polymer electrolyte membrane, Int. J. Hydrogen Energy 46 (42) (2021) 22040–22061.